J. Plasma Physics (1994), *vol.* 52, *part* 1, *pp.* 141–188
Copyright © 1994 Cambridge University Press

Steady MHD flows with an ignorable co-ordinate and the potential transonic flow equation

By G. M. WEBB,

Department of Planetary Sciences, University of Arizona, Tucson, Arizona 85721, U.S.A.

M. BRIO

Department of Mathematics, University of Arizona, Tucson, Arizona 85721, U.S.A.

AND G. P. ZANK

Bartol Research Institute, The University of Delaware, Newark, Delaware 19716, U.S.A.

(Received 3 March 1994)

The paper explores the interrelationship between the generalized Grad–Shafranov equation, or trans-field force balance equation, for steady MHD flows with an ignorable co-ordinate, and work by Imai on field-aligned MHD flows. The development of Imai, assumes at the outset that the fluid velocity **V** is parallel to the magnetic field **B**, and exploits an analogy with steady compressible irrotational flow in ordinary fluid dynamics. In Imai's analysis the magnetic induction **B** is written in the form $\mathbf{B} = \sigma\mathbf{b}$, where $\sigma \propto 1/(M_A^2 - 1)$, and M_A is the appropriate Alfvén Mach number. Gauss' law $\nabla.\mathbf{B} = \nabla.(\sigma\mathbf{b}) = 0$ then plays a role analogous to the mass continuity equation in ordinary fluid dynamics, where σ corresponds to the density of the pseudo-fluid. Imai's analysis leads to a transonic equation for the field potential ϕ defined by $\mathbf{b} = \nabla\phi$. For a restricted class of flows the trans-field force balance equation formulation also leads to the transonic potential flow equation, but the assumption of an ignorable co-ordinate allows for the possibility of non-field-aligned flows with non-zero electric field potential Φ_E. The characteristics of the generalized Grad–Shafranov equation are related to the Mach cone and the group velocity surface for linear magnetosonic waves. The corresponding forms of the characteristics for the potential transonic flow equation in the (x, y) plane and in the (b_x, b_y) hodograph plane are discussed. Sample solutions of the potential transonic flow equation for radial, helical and spiral flows are obtained by means of the hodograph transformation, and are used to illustrate the differences between hyperbolic and elliptic flows. The potential transonic flow equation is obtained for the case of an ignorable co-ordinate z of a rectangular Cartesian co-ordinate system (x, y, z), and also for the case of flows with an ignorable co-ordinate ϕ of a spherical polar co-ordinate system (r, θ, ϕ). Astrophysical applications are briefly discussed.

1. Introduction

Models of steady MHD flows have been used extensively to model stellar winds and jets (see e.g. Heinemann & Olbert 1978; Tsinganos 1981; Sakurai

1985, 1990; Hu & Low 1989; Heyvaerts & Norman 1989; Camenzind 1986, 1987), as well as models of bow shocks (see e.g. Spreiter, Summers & Alksne 1966; Spreiter, Summers & Rizzi 1970; Spreiter & Rizzi 1974). Most models assume the existence of an ignorable co-ordinate, allowing the reduction of the MHD equations to the trans-field force balance equation (or generalized Grad–Shafranov equation), coupled with a sequence of integrals (e.g. the Bernoulli integral, the angular momentum integral, and the entropy integral for flows that have an ignorable azimuthal co-ordinate ϕ in spherical polar co-ordinates). Work by Imai (1960) and Seebass (1961) showed that, for the case of field-aligned flows, the MHD equations could be reduced to the potential transonic flow equation of compressible irrotational fluid dynamics by the introduction of the notion of an equivalent non-magnetized pseudo-fluid. The main purpose of the present paper is to explore the conditions under which the trans-field force balance equation for flows with an ignorable co-ordinate may be reduced to the potential transonic flow equation. The analysis leads to some interesting solutions of the MHD equations that are useful for delineating the differences between hyperbolic and elliptic flows, as well as the differences between sub-Alfvénic and super-Alfvénic flows.

Section 2 introduces the steady MHD model employed. Section 3 considers the reduction of the MHD equations with an ignorable co-ordinate z of a rectangular Cartesian co-ordinate system to the trans-field force balance equation. A discussion of the characteristics of the trans-field equation reveals the conditions for the flow to be hyperbolic or elliptic. For hyperbolic flows the Mach angle between the characteristics and the projected flow direction on the (x, y) plane is determined, and the characteristics are related to the group velocity surface and Mach cone for linear magnetosonic waves. Section 4 shows the connection of the trans-field equation to the potential transonic flow equation for a class of flows for which the 'source' term in the trans-field force equation vanishes. The Mach number of the flow based on Imai's pseudo-fluid analogy, M, is shown to coincide with the Mach number of the flow based on the analysis of the characteristics of the generalized Grad–Shafranov equation. The characteristics of the potential transonic flow equation in the (b_x, b_y) hodograph plane are discussed. For the case where gravity may be neglected the characteristics in the hodograph plane can be integrated explicitly, and used to determine the simple wave solutions. Section 5 uses the hodograph transformation to obtain sample solutions of the potential transonic flow equation for the cases of radial flow, helical flow, and spiral flows about the z axis. The analysis extends the work of Seebass (1961) to include the role of non-zero components of the velocity, V_z and B_z, not included in Seebass' work. The representation of the flow and the characteristics in the hodograph plane are also discussed. In §6 the derivation of the trans-field equation for flows with an ignorable co-ordinate ϕ in spherical polar co-ordinates (r, θ, ϕ) is carried out. The reduction of the trans-field equation formulation to the potential transonic flow equation is then developed for this geometry. Section 7 concludes with a summary and discussion.

2. The model

The equations describing the steady inviscid flow of a high-electrical-conductivity MHD plasma consist of the dynamical equations for the gas, namely the mass continuity equation

$$\nabla . (\rho \mathbf{V}) = 0 \tag{2.1}$$

and the momentum equation

$$\rho \mathbf{V} . \nabla \mathbf{V} = \mathbf{J} \times \mathbf{B} - \rho \nabla \Phi_g - \nabla p, \tag{2.2}$$

supplemented by an appropriate equation of state relating the gas energy density to the entropy and density, and the Maxwell equations determining the inter-relationships between the electric field **E**, magnetic induction **B** and electric current density **J**. In the present analysis we assume that the first law of thermodynamics, or co-moving energy equation, is of the form

$$\mathbf{V} . \nabla (p/\rho^{\gamma}) = 0, \tag{2.3}$$

where γ is the polytropic index of the gas. The choice of the polytropic index γ in (2.3) may be used to simulate heat conduction if γ is smaller than the canonical value of the specific heat ratio γ_{ad}. In (2.1)–(2.3) ρ, p and **V** denote the gas density, pressure and velocity respectively, and Φ_g denotes the gravitational potential.

For a high-conductivity plasma $\mathbf{E} = -\mathbf{V} \times \mathbf{B}$, and Faraday's law in the MHD limit reduces to

$$\nabla \times \mathbf{E} \equiv -\nabla \times (\mathbf{V} \times \mathbf{B}) = 0. \tag{2.4}$$

The remaining Maxwell equations are Gauss' law

$$\nabla . \mathbf{B} = 0 \tag{2.5}$$

and Ampère's law

$$\mathbf{J} = \nabla \times \mathbf{B}/\mu, \tag{2.6}$$

where μ is the magnetic permeability.

The Maxwell equations (2.4)–(2.6) yield Poynting's theorem, or the electromagnetic energy equation in the form

$$\nabla . \left(\frac{\mathbf{E} \times \mathbf{B}}{\mu} \right) + \mathbf{J} . \mathbf{E} = 0, \tag{2.7}$$

whereas the co-moving energy equation (2.3) and continuity equation (2.1) may be used to write the gas energy equation in the form

$$\nabla . \left[\rho \mathbf{V} \frac{\gamma p}{(\gamma - 1) \rho} \right] - \mathbf{V} . \nabla p = 0. \tag{2.8}$$

Taking the scalar product of the momentum equation (2.2) with **V** and adding the resultant equation to (2.7) and (2.8) yields the total energy equation in the fixed reference frame as

$$\nabla . \left\{ \rho \mathbf{V} \left[\tfrac{1}{2} V^2 + \frac{\gamma p}{(\gamma - 1) \rho} + \Phi_g \right] + \frac{\mathbf{E} \times \mathbf{B}}{\mu} \right\} = 0, \tag{2.9}$$

where the terms from left to right represent the kinetic energy, enthalpy, gravitational and Poynting energy fluxes respectively.

3. Flows with an ignorable co-ordinate z

We now briefly review the reduction of the above equations for the case where all physical quantities are independent of an ignorable co-ordinate z of a rectangular Cartesian co-ordinate system using an analysis similar to that of Tsinganos (1981). In §3.1 we provide a reduction of the steady MHD equations to the trans-field force balance equation or generalized Grad–Shafranov equation, followed by a discussion of the characteristics and Mach cone for hyperbolic flows. In §3.2 we discuss the connection between the group velocity surface for linear magnetosonic waves (see e.g. Whitham 1974), the characteristics, the Mach cone, and the differences between hyperbolic and elliptic flows.

3.1. *The trans-field equation*

Since z is an ignorable co-ordinate, the condition $\nabla . \mathbf{B} = 0$ implies that the magnetic induction $\mathbf{B}$ may be expressed in the form

$$\mathbf{B} = \frac{\partial A}{\partial y}\mathbf{e}_x - \frac{\partial A}{\partial x}\mathbf{e}_y + B_z(x,y)\,\mathbf{e}_z \equiv \mathbf{B}_p + B_z\mathbf{e}_z. \tag{3.1}$$

Similarly, the mass continuity equation (2.1) implies that the fluid velocity $\mathbf{V}$ may be represented in the form

$$\mathbf{V} = \frac{1}{\mu\rho}\left(\frac{\partial\psi}{\partial y}\mathbf{e}_x - \frac{\partial\psi}{\partial x}\mathbf{e}_y\right) + V_z(x,y)\,\mathbf{e}_z \equiv \mathbf{V}_p + V_z\mathbf{e}_z. \tag{3.2}$$

As in the development by Tsinganos (1981), the analysis leads to a generalization of the Grad–Shafranov equation for the magnetic potential $A(x,y)$ that applies to steady flow situations. The magnetic field lines are described by the differential equations

$$\frac{dx}{\partial A/\partial y} = \frac{dy}{-\partial A/\partial x} = \frac{dz}{B_z}. \tag{3.3}$$

These equations integrate to yield $A(x,y) = \text{const.}$, for the projection of the field lines on the (x,y) plane. Similarly, the fluid streamlines have projections on the (x,y) plane described by the family of curves $\psi(x,y) = \text{const}$.

Equation (2.4) implies that the electric field $\mathbf{E}$ may be written as the gradient of a potential $\Phi_E(x,y)$ in the form

$$\mathbf{E} = -\mathbf{V}\times\mathbf{B} = -\nabla\Phi_E(x,y). \tag{3.4}$$

From (3.4), the z component of the electric field in the present model is zero. Using the representations (3.1) and (3.2) for $\mathbf{V}$ and $\mathbf{B}$, one finds from the z component of (3.4) that $E_z = -(\mu\rho)^{-1}\,\partial(\psi,A)/\partial(x,y) = 0$, from which it follows that $\psi = \psi(A)$. Also from (3.4),

$$\mathbf{E}.\mathbf{B} = -\nabla\Phi_E.\mathbf{B} = -\frac{\partial(\Phi_E,A)}{\partial(x,y)} = 0, \tag{3.5}$$

which implies that $\Phi_E \equiv \Phi_E(A)$ is solely a function of A. Since $\psi = \psi(A)$, (3.1) and (3.2) imply that the components of $\mathbf{V}$ and $\mathbf{B}$ in the (x,y) plane are given by

$$\mathbf{V}_p = \frac{\psi'(A)}{\mu\rho}\mathbf{B}_p = \frac{\alpha}{\rho}\mathbf{B}_p, \tag{3.6}$$

where the subscript p denotes components perpendicular to the z axis, and $\alpha \equiv \psi'(A)/\mu$, The (x, y) plane Alfvén Mach number of the flow, M_A, is defined by

$$M_A^2 = \frac{V_p^2}{V_{Ap}^2} = \frac{\mu\rho V_p^2}{B_p^2} = \frac{\mu\alpha^2}{\rho}, \tag{3.7}$$

where $\mathbf{V}_{Ap} = \mathbf{B}_p/(\mu\rho)^{\frac{1}{2}}$ is the (x, y) plane Alfvén velocity.

The component of (3.4) parallel to ∇A yields

$$V_z - \frac{\alpha}{\rho} B_z = \Phi_E'(A). \tag{3.8}$$

The z component of the momentum equation (2.2) leads to the vanishing-Jacobian condition $\partial(B_z - \psi'(A)\,V_z, A)/\partial(x, y) = 0$, which in turn implies the integral

$$V_z - \frac{B_z}{\psi'(A)} = \Lambda(A), \tag{3.9}$$

where $\Lambda(A)$ is an arbitrary function of A.

Equations (3.8) and (3.9) can be solved for V_z and B_z to obtain

$$V_z = \Phi_E'(A) + \frac{M_A^2(\Lambda - \Phi_E')}{M_A^2 - 1}, \tag{3.10}$$

$$B_z = \mu\alpha \frac{\Lambda - \Phi_E'(A)}{M_A^2 - 1}, \tag{3.11}$$

where M_A is the Alfvén Mach number defined in (3.7). These equations clearly display a possible Alfvén singularity as $M_A \to 1$. Furthermore, if $\Phi_E'(A) = 0$ then $V_z = (\alpha/\rho) B_z$, and the fluid velocity is then parallel to $\mathbf{B}$, with $\mathbf{V} = (\alpha/\rho)\,\mathbf{B}$. This latter case of field-aligned flow was considered by Imai (1960), whose analysis led to a potential transonic field equation similar to that occurring in steady irrotational fluid mechanics (see. e.g. Courant & Friedrichs 1948, chap. 4).

Two further integrals can be obtained in a straightforward fashion. The first of these is the polytropic integral

$$p = K(A)\,\rho^{\gamma}, \tag{3.12}$$

which follows from integrating the co-moving energy equation (2.3), where $K(A)$ is an arbitrary function of A. A further integral arises from the fixed-frame energy equation (2.9), namely

$$\tfrac{1}{2}V^2 + \frac{\gamma p}{(\gamma - 1)\rho} + \Phi_g - B_z \frac{\Phi_E'(A)}{\psi'(A)} = E(A), \tag{3.13}$$

where $E(A)$ is an arbitrary function of A.

It is of interest to note that the energy integral (3.13) may also be cast into the form

$$E_m(A) \equiv E + \tfrac{1}{2}[(\Lambda - \Phi_E')^2 - \Lambda^2] = \tfrac{1}{2}[V_p^2 + (V_z - \Phi_E')^2] + \frac{\gamma p}{(\gamma - 1)\rho} + \Phi_g. \tag{3.14}$$

Equation (3.14) corresponds to the energy integral in a reference frame Σ' moving with velocity $\mathbf{V}_t = \Phi_E'\,\mathbf{k}$ relative to the fixed frame. In the local frame Σ' the flow is field-aligned and the electric field and Poynting flux vanish.

The component of the momentum equation (2.2) parallel to ∇A yields the generalized Grad–Shafranov equation or trans-field equation

$$\frac{\alpha}{\rho}\left[\frac{\partial}{\partial x}\left(\frac{\alpha}{\rho}\frac{\partial A}{\partial x}\right)+\frac{\partial}{\partial y}\left(\frac{\alpha}{\rho}\frac{\partial A}{\partial y}\right)\right]-\frac{1}{\mu\rho}\left(\frac{\partial^2 A}{\partial x^2}+\frac{\partial^2 A}{\partial y^2}\right)=Q, \tag{3.15}$$

where

$$Q=E'(A)-K'(A)\frac{\rho^{\gamma-1}}{\gamma-1}+\frac{\alpha'}{\alpha}\frac{M_A^2(\Lambda-\Phi_E')^2}{(M_A^2-1)^2}-\Lambda\Lambda'-\frac{(\Lambda-\Phi_E')(\Lambda'-\Phi_E'')}{M_A^2-1}. \tag{3.16}$$

Equation (3.15) may be further analysed by noting that ρ is an implicit function of A, ∇A, x and y, obtained by solving the energy integral (3.13) for ρ. The derivatives $\partial\rho/\partial x$ and $\partial\rho/\partial y$ on the left-hand side of (3.15) may be obtained by differentiating the energy integral (3.13). The net result of this procedure is a second-order quasi-linear nonlinear partial differential equation for A, of the form

$$aA_{xx}+bA_{xy}+cA_{yy}+d=0, \tag{3.17}$$

where

$$\left.\begin{aligned} a&=\Delta-V_{px}^2V_p^2, \quad b=-2V_{px}V_{py}V_p^2,\\ c&=\Delta-V_{py}^2V_p^2, \quad \Delta=V_p^4-V_p^2(V_A^2+a_g^2)+V_{Ap}^2a_g^2, \end{aligned}\right\} \tag{3.18}$$

and $a_g=(\gamma p/\rho)^{\frac{1}{2}}$ and $V_A=B/(\mu\rho)^{\frac{1}{2}}$ are the gas sound speed and Alfvén speed respectively. The explicit form of the coefficient d is unwieldy, and is given in the appendix.

The characteristics of (3.17) are determined by solving the equation

$$F=a\xi_x^2+b\xi_x\xi_y+c\xi_y^2=0 \tag{3.19}$$

for $\xi(x,y)$. Solving (3.19) for ξ_y/ξ_x yields the equations

$$\xi_y=\zeta_\pm\,\xi_x, \tag{3.20}$$

where

$$\zeta_\pm=\frac{V_{px}V_{py}V_p^2\pm[\Delta(V_p^4-\Delta)]^{\frac{1}{2}}}{\Delta-V_{py}^2V_p^2}. \tag{3.21}$$

Thus the characteristics are real and (3.17) is hyperbolic provided that the discriminant

$$\delta=\Delta(V_p^4-\Delta)\equiv(V_A^2+a_g^2)(V_p^2-V_f^2)(V_p^2-V_s^2)(V_p^2-V_c^2), \tag{3.22}$$

is positive. In (3.22) the speeds V_f and V_s correspond to the phase speed of fast and slow magnetosonic waves propagating along $\mathbf{B}_p$. The speeds V_f and V_s are obtained by solving the equation $\Delta=0$ for V_p, namely

$$V_{f,s}^2=\tfrac{1}{2}\{V_A^2+a_g^2\pm[(V_A^2+a_g^2)^2-4V_{Ap}^2a_g^2]^{\frac{1}{2}}\}. \tag{3.23}$$

The speed V_c in (3.22) is given by

$$V_c=\frac{V_{Ap}a_g}{(V_A^2+a_g^2)^{\frac{1}{2}}}\equiv\frac{V_fV_s}{(V_f^2+V_s^2)^{\frac{1}{2}}}. \tag{3.24}$$

For the case where $B_z=0$, $V_A\equiv V_{Ap}$ and the speed V_c then coincides with the group velocity of the slow magnetosonic mode propagating perpendicular to $\mathbf{B}$ (i.e. $\mathbf{k}.\mathbf{B}=0$) at one of the slow-mode cusps. Since $V_f>V_s>V_c$, $\delta>0$ and

(3.17) is hyperbolic for V_p in the ranges $V_c < V_p < V_s$ and $V_p > V_f$. The parameter $\delta < 0$, and (3.17) is elliptic for V_p, in the ranges $0 < V_p < V_c$ and $V_s < V_p < V_f$. The first-order partial differential equations (3.20) for $\xi(x,y)$ have Cauchy characteristics

$$\frac{dy}{dx} = -\frac{1}{\zeta_{\pm}}. \tag{3.25}$$

The solutions of (3.25) for a given solution of (3.17) for $A(x,y)$ define characteristic curves $\xi(x,y) = \text{const.}$ and $\eta(x,y) = \text{const.}$ in the (x,y) plane.

To obtain further insight into the nature of the characteristics for the case of hyperbolic flows it is of interest to compute the Mach angle $\mathscr{A}$ between the characteristic direction $\hat{\xi} = \nabla\xi/|\nabla\xi|$ and the projected fluid velocity vector $\mathbf{V}_p$ via the formula

$$\sin^2\mathscr{A} = \frac{|\nabla\xi \times \mathbf{V}_p|^2}{V_p^2\,|\nabla\xi|^2}. \tag{3.26}$$

To compute $\mathscr{A}$, it is useful to note that the characteristic equation (3.19) may be cast in the form

$$F = (\Delta - V_p^4)\,|\nabla\xi|^2 + V_p^2\,|\nabla\xi \times \mathbf{V}_p|^2 = 0. \tag{3.27}$$

From (3.26) and (3.27), we deduce that

$$\sin^2\mathscr{A} = \frac{1}{M^2}, \tag{3.28}$$

where we identify

$$M^2 = \frac{V_p^4}{V_p^4 - \Delta} \tag{3.29}$$

as the square of the effective Mach number of the flow. Equation (3.28) is analogous to the formula for the Mach cone angle $\mathscr{A}$ for supersonic flow past a stationary object emitting sound waves in ordinary gasdynamics (see e.g. Landau & Lifshitz 1987), in which the sound-wave disturbances are confined to the Mach cone.

From (3.29), we find

$$M^2 - 1 = \frac{(V_p^2 - V_f^2)\,(V_p^2 - V_s^2)}{(V_A^2 + a_g^2)\,(V_p^2 - V_c^2)}. \tag{3.30}$$

For hyperbolic flow $M^2 > 1$, and the flow is 'sonic' (i.e. $M = 1$) when the flow speed V_p matches either the fast or slow magnetosonic speeds V_f or V_s.

An alternative form of the characteristic equation (3.19) may be obtained by converting to polar co-ordinates (r,Θ), where $(x,y) = r(\cos\Theta, \sin\Theta)$ gives the position vector in the (x,y) plane. In terms of r and Θ, (3.19) assumes the form

$$(\Delta - V_p^2\,V_r^2)\,\xi_r^2 - 2V_p^2\frac{V_r V_\Theta}{r}\xi_r\,\xi_\Theta + \frac{\Delta - V_p^2\,V_\Theta^2}{r^2}\xi_\Theta^2 = 0. \tag{3.31}$$

This form of the characteristics is of interest in the consideration of the radial, helical and spiral flows considered in §5.

In terms of the characteristic co-ordinates (ξ,η) obtained by solving (3.20) and (3.25), the generalized Grad–Shafranov equation (3.17) reduces to the canonical form

$$\Gamma A_{\xi\eta} + l(\xi)A_\xi + l(\eta)A_\eta + d = 0, \tag{3.32}$$

where

$$\Gamma = \frac{4\xi_x \xi_y \Delta(\Delta - V_p^4)}{\Delta - V_{py}^2 V_p^2}, \tag{3.33}$$

$$l(\xi) = a\xi_{xx} + b\xi_{xy} + c\xi_{yy}. \tag{3.34}$$

Equation (3.32) is the canonical form of the Grad–Shafranov equation in characteristic co-ordinates (ξ, η) applicable for hyperbolic flows.

3.2. *The group velocity surface and Mach cone*

In this section our aim is to shed light on the nature of the characteristics (3.20) for hyperbolic flows, and the Mach cone described by (3.28) and (3.29), by a consideration of the group velocity surface for linear magnetosonic waves. We restrict the discussion to the case of field-aligned flows confined to the (x, y) plane. Related ideas on the characteristics for hyperbolic MHD flows are discussed by Sears (1960), Jeffrey & Taniuti (1964) and Polovin & Demutskii (1990) and references therein. We first discuss the group velocity surface for linear magnetosonic waves in a stationary medium using the approach of Whitham (1974) (see also Webb *et al.* 1993), and then go on to discuss the group velocity for magnetosonic waves in a steady flow and the Mach cone.

3.2.1. *The group velocity surface*

The propagation of linear magnetosonic waves in a stationary background medium is described by the wave equation

$$\mathscr{L}(\varphi) = \left[\frac{\partial^4}{\partial t^4} - (V_A^2 + a_g^2)\frac{\partial^2}{\partial t^2}\nabla^2 + V_A^2 a_g^2 \frac{\partial^2}{\partial x_1^2}\nabla^2\right]\varphi = 0. \tag{3.35}$$

where φ for example represents the density perturbation (Lighthill 1960; Whitham 1974; McKenzie 1991). Here x_1 denotes distance along the uniform background magnetic field direction. Plane waves with perturbation $\varphi \propto \exp[i(\mathbf{k}.\mathbf{x} - \omega t)]$ from (3.35) satisfy the magnetosonic dispersion equation

$$\omega^4 - (V_A^2 + a_g^2)\,\omega^2 k^2 + V_A^2 a_g^2 k_{x_1}^2 k^2 = 0. \tag{3.36}$$

By using the identifications

$$\omega = -S_t, \quad \mathbf{k} = \nabla S, \tag{3.37}$$

where S is the wave phase, we obtain the wave eikonal equation

$$S_t^4 - (V_A^2 + a_g^2) S_t^2 (\nabla S)^2 + V_A^2 a_g^2 S_{x_1}^2 (\nabla S)^2 = 0. \tag{3.38}$$

This equation arises naturally in WKB expansions for MHD wave propagation, and plays a central role in defining the group velocity surface or eikonal surface for magnetosonic waves.

Next we introduce cylindrical spatial co-ordinates about the magnetic field such that $\mathbf{r} = (x_1, x_2\cos\phi, x_2\sin\phi)$, and co-ordinates $\mathbf{k} = k(\cos\vartheta, \sin\vartheta\cos\Phi, \sin\vartheta\sin\Phi)$ in $\mathbf{k}$ space ($\mathbf{k} = \nabla S$). The wave eikonal equation (3.38) has a complete integral in the form of a plane wave

$$S = k[x_1\cos\vartheta + x_2\sin\vartheta - c(\vartheta)\,t] + S_0, \tag{3.39}$$

where k, ϑ and S_0 are regarded as arbitrary constants, and $c(\vartheta) = \omega/k$ is the phase speed of the wave, satisfying the magnetosonic dispersion equation

$$c^4 - (V_A^2 + a_g^2)\,c^2 + V_A^2 a_g^2 \cos^2\vartheta = 0. \tag{3.40}$$

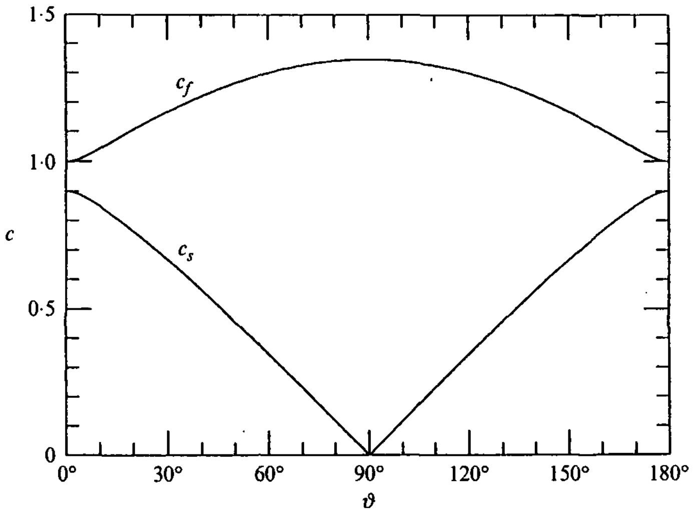

FIGURE 1. Fast and slow magnetosonic wave speeds c_f and c_s versus wave normal angle ϑ between **k** and $\mathbf{B}_0$ for the case $a = 1$ and $b = 0{\cdot}9$.

Since $\omega = c(\vartheta)\,k$, the group velocity of the wave $\mathbf{V}_g$ is given by

$$\mathbf{V}_g = \frac{\partial\omega}{\partial\mathbf{k}} = c(\vartheta)\,\mathbf{e}_k + c'(\vartheta)\,\mathbf{e}_\vartheta, \tag{3.41}$$

where

$$\mathbf{e}_k = \cos\vartheta\,\mathbf{e}_1 + \sin\vartheta\,\mathbf{e}_2, \tag{3.42}$$

$$\mathbf{e}_\vartheta = -\sin\vartheta\,\mathbf{e}_1 + \cos\vartheta\,\mathbf{e}_2, \tag{3.43}$$

are unit vectors in the **k** and ϑ directions respectively.

The group velocity surface for the waves $\mathbf{r} = \mathbf{V}_g t$ can be constructed simply from (3.41)–(3.43) in the parametric form

$$\left.\begin{aligned} x_1 &= V_{g1}t = [c(\vartheta)\cos\vartheta - c'(\vartheta)\sin\vartheta]\,t, \\ x_2 &= V_{g2}t = [c'(\vartheta)\cos\vartheta + c(\vartheta)\sin\vartheta]\,t \end{aligned}\right\} \tag{3.44}$$

by varying the wave normal angle ϑ. An alternative instructive way of constructing the group velocity surface described by (3.44) is to note that the wave eikonal equation (3.38) possesses a general integral as an envelope of plane waves for different ϑ (Sneddon 1957). This general solution is obtained by determining $\vartheta = \vartheta(x_1, x_2, t)$ from the envelope equation $S_\vartheta = 0$, and then substituting this value of ϑ into the particular integral (3.39). Taking $S_0 = 0$, the simultaneous solution of the equations $S = 0$ and $S_\vartheta = 0$ in the solution (3.39) yields the wave front (3.44) for a point source as an envelope of 'plane' waves. Thus the group velocity surface (3.44) may be thought of as an envelope of plane waves.

Using the notation

$$a \equiv \max\{V_A, a_g\}, \quad b \equiv \min\{V_A, a_g\}, \tag{3.45}$$

figure 1 shows the variation of the fast and slow magnetosonic wave speeds c_f and c_s obtained by solving (3.40) as

$$c_{f,s}^2 = \tfrac{1}{2}\{a^2 + b^2 \pm [(a^2+b^2)^2 - 4a^2b^2\cos^2\vartheta]^{\frac{1}{2}}\}, \tag{3.46}$$

as functions of ϑ for the case $a = 1$ and $b = 0.9$.

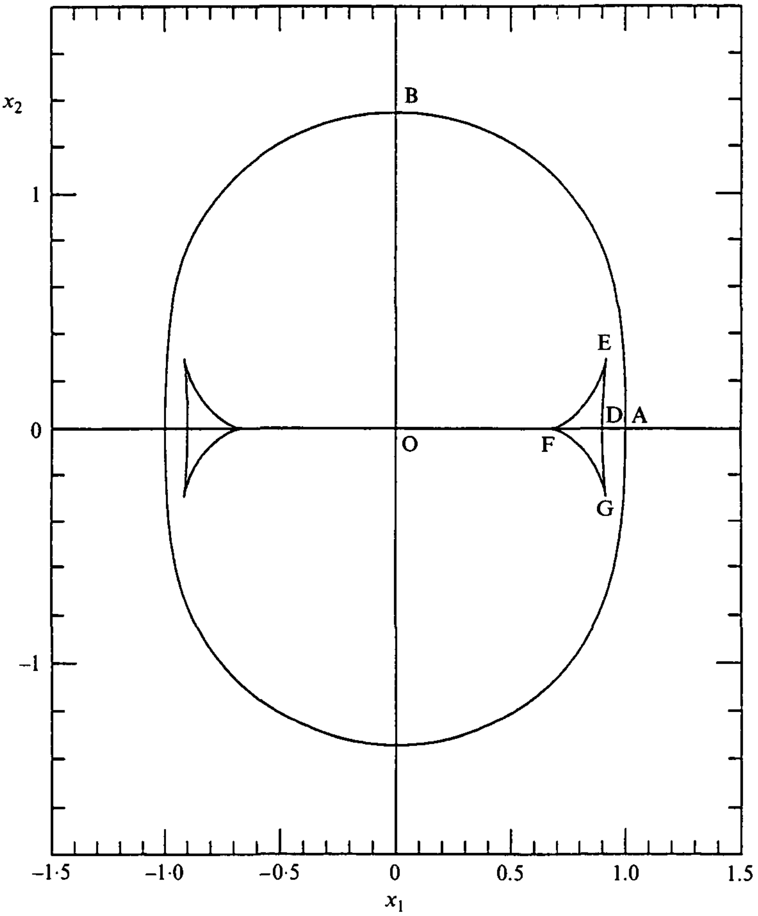

FIGURE 2. Fast and slow magnetosonic wave eikonal or group velocity surfaces for $a = 1$, $b = 0{\cdot}9$ and $t = 1$.

Figure 2 shows the group velocity surface described by (3.44) for fast and slow magnetosonic waves for $a = 1$ and $b = 0{\cdot}9$. The group velocity is in the direction of the straight line vector $\mathbf{OP} = \mathbf{V}_g t$ from the origin to a point $P(x_1, x_2)$ on the wave eikonal surface. The wave vector $\mathbf{k}$ is normal to the surface. Taking $S_0 = 0$, the straight lines $S = 0$ described by (3.39) are tangent to the group velocity surface.

3.2.2. *The Mach cone*

To construct the Mach cone for supersonic flows, it suffices to determine the group velocity vector field

$$\mathbf{V}_g = \tilde{\mathbf{V}}_g + \mathbf{V} \tag{3.47}$$

for magnetosonic waves at a fixed point in the flow, where $\tilde{\mathbf{V}}_g$ denotes the group velocity of the waves in the fluid frame. In (3.47) $\mathbf{V}$ denotes the fluid velocity vector. In order to illustrate the general ideas, and to simplify the mathematics, we consider only the case of field-aligned MHD flow in the (x, y) plane. Hence the velocity field $\mathbf{V} = V_p \mathbf{e}_1$ is taken parallel to the magnetic field $\mathbf{B} \equiv \mathbf{B}_p$ in the (x, y) plane.

The Mach cone construction is illustrated in figure 3, which displays the group velocity surface $\tilde{\mathbf{r}} = \tilde{\mathbf{V}}_g$ in the fluid frame for the fast magnetosonic mode (we take $t = 1$ in the time-dependent formulae of §3.2.1). The group velocity of the waves in the fixed frame is obtained from the vector addition of $\tilde{\mathbf{V}}_g$ and $\mathbf{V}$ via the Galilean transformation (3.47). Magnetosonic disturbances originating at the point Q in the flow are confined to the Mach cone $\mathrm{P_1QP_2}$, where the limiting edge of the Mach cone $\mathrm{P_1Q}$ is tangent to the group velocity surface.

The first obvious geometrical aspect of the Mach cone from figure 3 is that the Mach cone angle $\mathscr{A}$ and the wave normal angle ϑ on the Mach cone are related by

$$\vartheta + \mathscr{A} = \tfrac{1}{2}\pi, \tag{3.48}$$

a result that follows immediately from the fact that the wave vector $\mathbf{k}$ is perpendicular to $\mathbf{V}_g$ on the Mach cone.

From (3.39), the equation of the tangent $\mathrm{P_1Q}$ to the Mach cone is described by the equation

$$S = x_1 \cos\vartheta + x_2 \sin\vartheta - c(\vartheta) = 0, \tag{3.49}$$

obtained by setting $S_0 = 0$ and $t = 1$ in (3.39). Setting $x_2 = 0$ in (3.49) and solving the resulting equation for x_1, we deduce that the vector **QO** representing the fluid velocity $\mathbf{V}_p$ has magnitude

$$|\mathrm{QO}| = V_p = \frac{c}{\cos\vartheta}. \tag{3.50}$$

Equations (3.48) and (3.50) now yield the basic formula

$$\sin\mathscr{A} = \frac{1}{M}, \tag{3.51}$$

for the Mach cone angle $\mathscr{A}$, where

$$M = \frac{V_p}{c} \tag{3.52}$$

is the Mach number of the flow based on the magnetosonic speed $c(\vartheta)$ as measured on the Mach cone. The phase speed $c(\vartheta)$ of the magnetosonic waves of interest on the Mach cone may be determined from the formula $\cos\vartheta = c/V_p$ for the wave normal angle ϑ from (3.50), and from the dispersion equation (3.40), to obtain

$$c^2 = V_A^2 + a_g^2 - \frac{V_A^2 a_g^2}{V_p^2}. \tag{3.53}$$

Combining (3.52) and (3.53) yields the result

$$M^2 = \frac{V_p^4}{V_p^4 - \Delta} \tag{3.54}$$

for the square of the effective Mach number of the flow, where Δ is defined in (3.18) with $V_A \equiv V_{Ap}$. Hence the analysis of the Mach cone based on the group velocity surface leads to the basic formulae (3.28) and (3.29) for the Mach cone angle $\mathscr{A}$ obtained previously from an analysis of the characteristics of the generalized Grad–Shafranov equation (3.17).

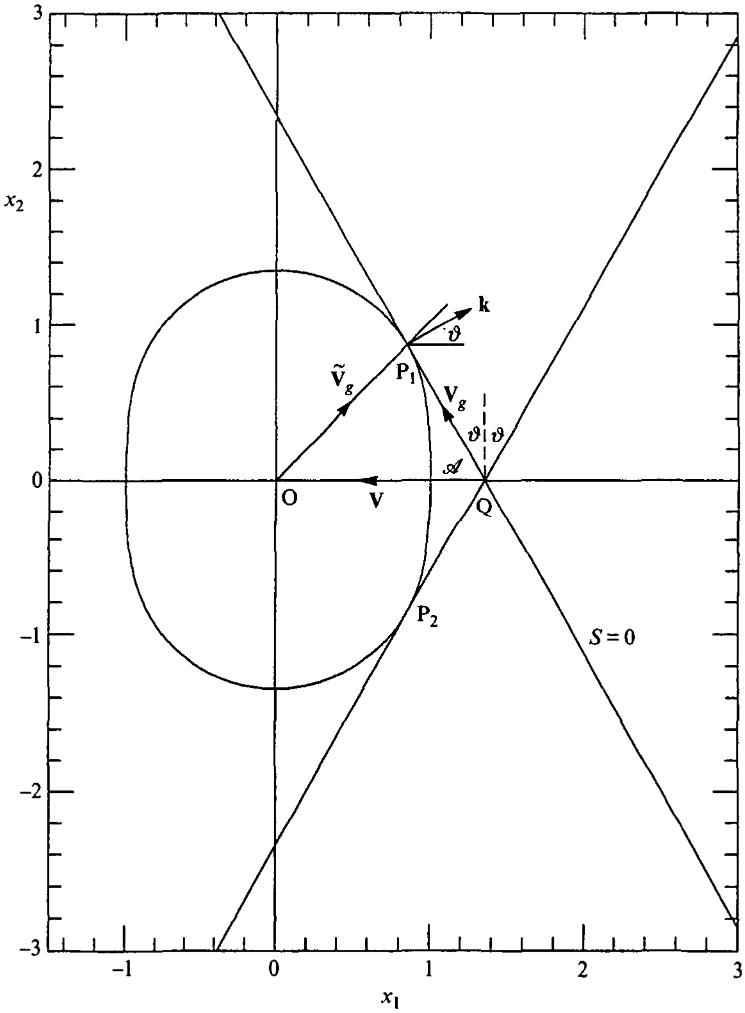

FIGURE 3. Construction of the Mach cone for the case of field-aligned flow in the (x, y) plane for hyperbolic flows with $V_p > V_f$.

To determine the group velocity $\mathbf{V}_g$ on the Mach cone, we note from (3.44) and (3.47) that

$$\mathbf{V}_g = [c\cos\vartheta - c'(\vartheta)\sin\vartheta - V_p]\,\mathbf{e}_1 + [c'(\vartheta)\cos\vartheta + c\sin\vartheta]\,\mathbf{e}_2. \tag{3.55}$$

The unit vectors $\mathbf{e}_1$ and $\mathbf{e}_2$ are given by

$$\mathbf{e}_1 = (A_y, -A_x, 0)/B_p, \quad \mathbf{e}_2 = (A_x, A_y, 0)/B_p. \tag{3.56}$$

Noting that $\mathbf{V}_p = (\alpha/\rho)\,\mathbf{B}_p$ from (3.6), we obtain the formulae

$$\left.\begin{aligned} V^{\pm}_{gx} &= -\Lambda[V_x(M^2-1)^{\frac{1}{2}} \pm V_y], \\ V^{\pm}_{gy} &= -\Lambda[V_y(M^2-1)^{\frac{1}{2}} \mp V_x] \end{aligned}\right\} \tag{3.57}$$

for the group velocity components on the Mach cone, where

$$\Lambda = \frac{(V_p^4-\Delta)^{\frac{3}{2}}\,\Delta^{\frac{1}{2}}}{V_p^4\,[(V_A^2+a_g^2)\,V_p^2 - 2V_A^2\,a_g^2]}. \tag{3.58}$$

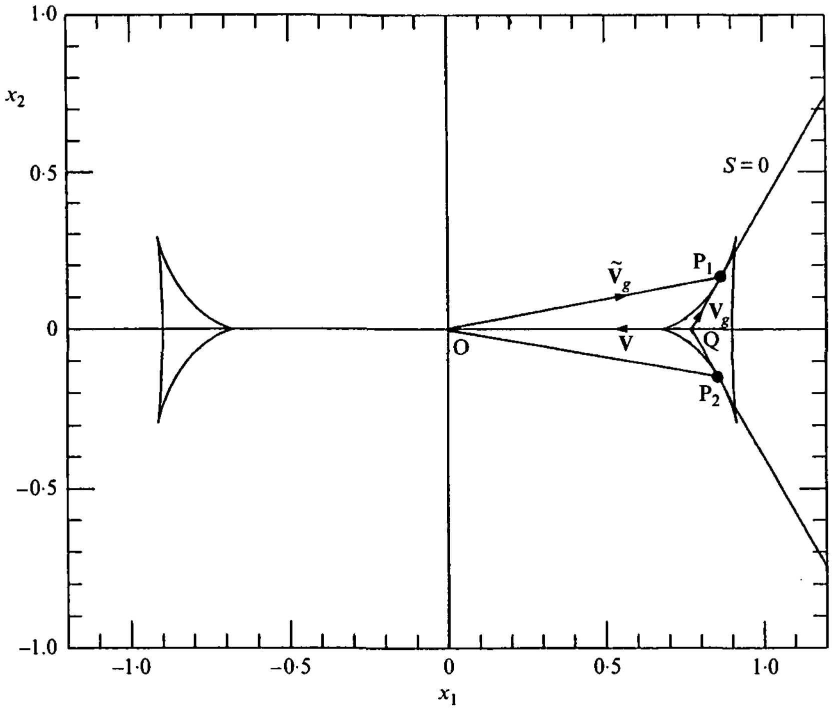

FIGURE 4. Construction of the Mach cone for the case of sub-Alfvénic field-aligned flow in the (x, y) plane in which the fluid speed lies in the hyperbolic flow regime $V_c < V_p < V_s$.

Equations (3.57) may be used to show that the group velocity directions on the Mach cone coincide with the characteristic directions described by (3.20) and (3.21). A straightforward computation shows that

$$\lambda_\pm = \frac{V^\pm_{gy}}{V^\pm_{gx}} = \zeta_\mp , \tag{3.59}$$

where $\xi_y/\xi_x = \zeta_\pm$ determines the characteristic directions for the generalized Grad–Shafranov equation (3.17).

The Mach cone illustrated in figure 3 corresponds to a super-fast magnetosonic flow with $V_p > V_f \equiv \max(V_A, a_g)$, in which the Mach cone occupies the region downstream of the source point Q of the waves. One can also construct a Mach cone for the slow magnetosonic flow regime $V_c < V_p < V_s$, where $V_s = \min(V_A, a_g)$, illustrated in figure 4. In this case the Mach cone $\mathrm{P}_1\mathrm{Q}\mathrm{P}_2$ extends upstream of the wave source Q. It is not possible to construct a Mach cone in the elliptic flow regimes $V_s < V_p < V_f$ and $0 < V_p < V_c$, since the characteristics are then complex.

A similar analysis of the Mach cone can clearly be carried out for flows not restricted to the (x, y) plane, but in this more general case the analysis is complicated by the fact that the waves of interest have their **k** vector restricted to the (x, y) plane, whereas **B** and **V** have components outside the (x, y) plane.

4. The potential transonic flow equation

In this section we show the connection between Imai's analysis of field-aligned MHD flow and the generalized Grad–Shafranov equation (3.15). The potential transonic flow equation is derived in §4.1 for the case of flows with an ignorable co-ordinate z of a rectangular Cartesian co-ordinate system (x, y, z). The characteristics of the potential transonic flow equation in both the (x, y) plane and the (b_x, b_y) hodograph plane are obtained in §4.2.

4.1. *The potential transonic flow equation*

Taking into account

$$\nabla\times\mathbf{V}_p=-\left[\frac{\partial}{\partial x}\left(\frac{\alpha}{\rho}\frac{\partial A}{\partial x}\right)+\frac{\partial}{\partial y}\left(\frac{\alpha}{\rho}\frac{\partial A}{\partial y}\right)\right]\mathbf{e}_z,\quad \nabla\times\mathbf{B}_p=-\left(\frac{\partial^2 A}{\partial x^2}+\frac{\partial^2 A}{\partial y^2}\right)\mathbf{e}_z,\tag{4.1}$$

the generalized Grad–Shafranov equation (3.15) may be written in the form

$$\nabla\times[(1-M_A^2)\mathbf{B}_p].\mathbf{e}_z=\mu\rho Q+\frac{\mu\alpha B_p^2}{\rho}\frac{d\alpha}{dA}.\tag{4.2}$$

An inspection of the form of Q in (3.16) reveals that $Q=0$ for the special class of flows for which

$$\alpha'=0,\quad E'-\Lambda\Lambda'=0,\quad K'=0,\quad \Lambda'-\Phi_E''=0,\tag{4.3}$$

and (4.2) is then equivalent to

$$\nabla\times\mathbf{b}=0,\tag{4.4}$$

where

$$\mathbf{b}=\frac{(1-M_A^2)\mathbf{B}_p}{(1-M_{A0}^2)B_{p0}}\equiv\frac{1}{\sigma}\frac{\mathbf{B}_p}{B_{p0}},\quad \sigma=\frac{1-M_{A0}^2}{1-M_A^2},\tag{4.5}$$

and M_{A0} and B_{p0} denote constant reference values of M_A and B_p. In terms of $\mathbf{b}$, Gauss' law $\nabla.\mathbf{B}=0$ assumes the form

$$\nabla.(\sigma\mathbf{b})=0.\tag{4.6}$$

Equations (4.4) and (4.6) are analogous to the equations of steady irrotational compressible fluid flow in which $\mathbf{b}$ plays the role of the fluid velocity and σ the role of the density. This analogy was first noted by Imai (1960), who considered the case of field-aligned flow. The present analysis indicates that this analogy also holds for cases including gravity ($\Phi_g\neq 0$) and for non-field-aligned flows, which occur in the presence of a non-zero electric field ($\Phi_E'\neq 0$; see (3.10) and (3.11)). We note that the class of flows for which the conditions (4.3) hold includes the case where E, K, α, Λ and Φ_E' are constant throughout the flow. Equations (3.10) and (3.11) also reveal that the choice $\Lambda=\Phi_E'$ corresponds to a flow with $B_z=0$, and $V_z=\Phi_E'(A)$. This latter flow is free of the Alfvén singularity for V_z and B_z. More generally, (4.3) may be integrated to yield

$$\alpha=\alpha_0,\quad E-\tfrac{1}{2}\Lambda^2=E_0-\tfrac{1}{2}\Lambda_0^2,\quad K=K_0,\quad \Lambda-\Phi_E'=\Lambda_0-\Phi_{E0}',\tag{4.7}$$

where quantities with subscript 0 on the right-hand sides of (4.7) are integration constants. If $\Lambda_0-\Phi_{E0}'\neq 0$ then V_z and B_z exhibit a singularity at the Alfvén point $M_A=1$.

For non-magnetized fluid flows, the energy conservation or Bernoulli integral (3.13) is of the form

$$\tfrac{1}{2}V^2+\int\frac{dp}{\rho}+\Phi_g=E, \tag{4.8}$$

from which it follows that the adiabatic sound speed $a_g=(\partial p/\partial\rho)^{\frac{1}{2}}$ satisfies the equation

$$a_g^2=-\rho V\left(\frac{\partial V}{\partial\rho}\right)_{\Phi_g}. \tag{4.9}$$

Hence for the pseudo-fluid described by (4.4) and (4.6) one may identify the square of the effective sound speed, a^2, as

$$a^2=-\sigma b\left(\frac{\partial b}{\partial\sigma}\right)_{\Phi_g}. \tag{4.10}$$

We note for later reference from (4.5) that

$$\frac{d\rho}{d\sigma}=\frac{\rho(M_A^2-1)}{\sigma M_A^2}. \tag{4.11}$$

To compute a^2, we first note that the energy integral E from (3.13) may be written in the form

$$E=\frac{\alpha^2}{2\rho^2}B_p^2+\frac{\mu^2\alpha^4(\Lambda-\Phi_E')^2}{2(\mu\alpha^2-\rho)^2}+\frac{\gamma}{\gamma-1}K\rho^{\gamma-1}+\Phi_g+\Phi_E'(\Lambda-\tfrac{1}{2}\Phi_E'). \tag{4.12}$$

In view of the conditions (4.3) imposed on E, α, Λ, K and Φ_E' in the present analysis, differentiation of (4.12) yields

$$0\equiv(E'-\Lambda\Lambda')\,dA=V_p^2\left[\left(\frac{1}{M_A^2}+\frac{M_A^2-1}{M_A^2M_s^2}+\frac{V_{Az}^2}{V_p^2}\right)\frac{d\sigma}{\sigma}+\frac{db}{b}+\frac{d\Phi_g}{V_p^2}\right], \tag{4.13}$$

where $M_s=V_p/a_g$ is the sonic Mach number and $a_g=(\gamma p/\rho)^{\frac{1}{2}}$ the gas sound speed. The left-hand side of (4.13) is zero by the assumption $E'-\Lambda\Lambda'=0$ in (4.3). From (4.10) and (4.13), we find

$$a^2=\frac{b^2}{V_p^4}(V_p^4-\Delta),\quad M^2=\frac{b^2}{a^2}=\frac{V_p^4}{V_p^4-\Delta} \tag{4.14}$$

for the effective pseudo-fluid sound speed a and Mach number M, where Δ is defined in (3.18). From (4.14), the square of the pseudo-fluid Mach number $M^2=b^2/a^2$ is given by (3.29), which is just the square of the Mach number based on the characteristics (3.27) and Mach cone of the generalized Grad–Shafranov equation (3.17). Thus, from (3.30), the pseudo-fluid flow, like the Grad–Shafranov equation flow, is hyperbolic in the regions where $M^2>1$, namely $V_p>V_f$ and $V_c<V_p<V_s$, but is elliptic for V_p in the ranges $0<V_p<V_c$ and $V_s<V_p<V_f$. The Mach number M may also be expressed in the form

$$M^2=\frac{M_A^2M_s^2}{M_s^2+M_A^2-1+M_A^2M_s^2/M_{Az}^2},\quad M_{Az}^2=\frac{V_p^2}{V_{Az}^2}. \tag{4.15}$$

The continuity equation (4.6) for **b** can now be reduced to the transonic potential flow equation. First note that (4.6) may be written as

$$\sigma\left(\frac{\partial b_x}{\partial x}+\frac{\partial b_y}{\partial y}\right)+b_x\frac{\partial \sigma}{\partial x}+b_y\frac{\partial \sigma}{\partial y}=0. \tag{4.16}$$

However, from (4.13),

$$\left.\begin{aligned}\frac{\partial \sigma}{\partial x}&=-\sigma\left[\frac{1}{a^2}\left(b_x\frac{\partial b_x}{\partial x}+b_y\frac{\partial b_y}{\partial x}\right)+\frac{M^2}{V_p^2}\frac{\partial \Phi_g}{\partial x}\right],\\ \frac{\partial \sigma}{\partial y}&=-\sigma\left[\frac{1}{a^2}\left(b_x\frac{\partial b_x}{\partial y}+b_y\frac{\partial b_y}{\partial y}\right)+\frac{M^2}{V_p^2}\frac{\partial \Phi_g}{\partial y}\right].\end{aligned}\right\} \tag{4.17}$$

Substitution of the results (4.17) into (4.16) results in the equation

$$(a^2-b_x^2)\frac{\partial b_x}{\partial x}+(a^2-b_y^2)\frac{\partial b_y}{\partial y}-b_x b_y\left(\frac{\partial b_y}{\partial x}+\frac{\partial b_x}{\partial y}\right)-\frac{b^2}{V_p^2}\mathbf{b}.\nabla\Phi_g=0. \tag{4.18}$$

Since $\nabla\times\mathbf{b}=0$, **b** must also satisfy the equation

$$\frac{\partial b_y}{\partial x}-\frac{\partial b_x}{\partial y}=0. \tag{4.19}$$

A natural way to incorporate the condition $\nabla\times\mathbf{b}=0$ is to write **b** as the gradient of a potential in the form $\mathbf{b}=\nabla\phi$, so that (4.18) reduces to

$$(a^2-\phi_x^2)\,\phi_{xx}+(a^2-\phi_y^2)\,\phi_{yy}-2\phi_x\,\phi_y\,\phi_{xy}-\frac{\phi_x^2+\phi_y^2}{V_p^2}\nabla\phi.\nabla\Phi_g=0. \tag{4.20}$$

Equation (4.20) is the usual transonic flow equation for non-magnetized compressible irrotational flow in the presence of gravity (see e.g. Courant & Friedrichs 1948, chap. 4; von Mises 1958, chaps 2 and 4).

There is an extensive literature on the irrotational fluid equations (4.18) and (4.19) and the potential transonic flow equation (4.20) in the case where the gravitational force is negligible, since in this case (4.18) and (4.19) may be linearized by the hodograph transformation, by interchanging the role of the dependent and independent variables. Writing $(b_x, b_y, 0)=(u, v, 0)$, one finds for $\Phi_g=0$ that the hodograph transformation yields a linearization of the equations provided that the Jacobian of the transformation is non-zero:

$$j=\frac{\partial(u,v)}{\partial(x,y)}\equiv\frac{\partial(b_x,b_y)}{\partial(x,y)}\neq 0. \tag{4.21}$$

For $j=0$, one obtains the so-called simple-wave solutions. Some simple applications of (4.18) and (4.19) to 'magnetic source' and 'magnetic vortex' flow for field-aligned flow that uses the hodograph transformation and Chaplygin's equation are given by Seebass (1961).

Below, we discuss the characteristics of (4.18) and (4.19).

4.2. *The characteristic equations*

The characteristics of (4.18) and (4.19) in the (x, y) plane in the hyperbolic regime consist of two families of curves $C^-:\alpha(x,y)=\text{const.}$, and $C^+:\beta(x,y)=\text{const}$, satisfying the equation

$$a^2|d\mathbf{r}|^2-|\mathbf{b}\times d\mathbf{r}|^2=0, \tag{4.22}$$

where $d\mathbf{r} = (dx, dy, 0)$ is the differential in the characteristic direction. Thus the curves C^+ and C^- satisfy the differential equations

$$C^+: \quad \frac{dy}{d\alpha} = \zeta_+ \frac{dx}{d\alpha}, \tag{4.23}$$

$$C^-: \quad \frac{dy}{d\beta} = \zeta_- \frac{dx}{d\beta}, \tag{4.24}$$

where

$$\zeta_\pm = \frac{b_x b_y \pm a(b^2 - a^2)^{\frac{1}{2}}}{b_x^2 - a^2} \tag{4.25}$$

(Courant & Friedrichs 1948, chap. 2, §23, p. 47). From the characteristic equations in the form (4.22), the Mach angle $\mathscr{A}$ between the flow $\mathbf{b}$ and the characteristics is given by the equation

$$\sin^2 \mathscr{A} = \frac{|\mathbf{b} \times d\mathbf{r}|^2}{b^2 |d\mathbf{r}|^2} = \frac{1}{M^2}. \tag{4.26}$$

Thus, perhaps as might have been expected, the Mach angle for the pseudo-flow is just the same as for the Grad–Shafranov flow. The Mach angle $\mathscr{A} \to 0$ and the characteristics are nearly aligned with the projected streamlines on the (x, y) plane as $M \to \infty$ (i.e. for $V_p \gg V_f$ and also as $V_p \downarrow V_c$). Similarly, as $V_p \to V_f$ or as $V_p \to V_s$, one has $M \to 1$ and $\mathscr{A} \to 90°$, and the projected streamlines and characteristics are nearly orthogonal for weakly supersonic flows.

The corresponding form of the characteristics Γ^+ and Γ^- in the (b_x, b_y) plane are

$$\Gamma^+: \quad \frac{db_x}{d\alpha} = -\zeta_- \frac{db_y}{d\alpha} + \frac{b^2}{a^2 - b_x^2} \frac{\mathbf{b}.\nabla\Phi_g}{V_p^2} \frac{dx}{d\alpha}, \tag{4.27}$$

$$\Gamma^-: \quad \frac{db_x}{d\beta} = -\zeta_+ \frac{db_y}{d\beta} + \frac{b^2}{a^2 - b_x^2} \frac{\mathbf{b}.\nabla\Phi_g}{V_p^2} \frac{dx}{d\beta}. \tag{4.28}$$

An alternative form of the characteristic equations (4.27) and (4.28) is

$$a^2 |d\mathbf{b}|^2 - |\mathbf{b}.d\mathbf{b}|^2 - \frac{b^2(\mathbf{b}.\nabla\Phi_g)}{V_p^2} d\mathbf{r}.d\mathbf{b} = 0, \tag{4.29}$$

where $d\mathbf{b} = (db_x, db_y, 0)$ and $d\mathbf{r} = (dx, dy, 0)$.

One can regard the characteristic equations (4.23), (4.24) and (4.27), (4.28) as four partial differential equations for x, y, b_x and b_y as functions of α and β, provided that the transformation of co-ordinates from $(x, y) \to (\alpha, \beta)$ is non-singular. The curves $\alpha(x, y) = \text{const}$ and $\beta(x, y) = \text{const}$ in the (x, y) plane may then be identified with the characteristics C^- and C^+ respectively.

In the absence of gravity ($\Phi_g = 0$), one can show that the characteristics C^+ and Γ^-, and the characteristics C^- and Γ^+ are mutually orthogonal. For $\Phi_g = 0$, (4.18) and (4.19) are reducible in the sense that the characteristics Γ^+ and Γ^-, (4.27) and (4.28), then depend only on b_x and b_y, and hence can be integrated. From the energy integral (4.12), b, a and M depend only on the density ρ, so that

$b = b(\rho)$, $a = a(\rho)$ and $M = M(\rho)$. Inverting the relation $b = b(\rho)$ then implies that $a = a(b)$ and $M = M(b)$ Using these facts and converting to polar co-ordinates in the (b_x, b_y) plane leads to the solution of the characteristics Γ^+ and Γ^- as

$$\Gamma^+ : \quad \theta - \int^b (M^2-1)^{\frac{1}{2}} \frac{db}{b} = \beta = \text{const}, \tag{4.30}$$

$$\Gamma^- : \quad \theta + \int^b (M^2-1)^{\frac{1}{2}} \frac{db}{b} = \alpha = \text{const}. \tag{4.31}$$

Equations (4.30) and (4.31) thus lead to the identification of the characteristic co-ordinates α and β. Γ^+ simple-wave solutions correspond to flows in which β is constant throughout the region of the (x, y) plane of interest. Similarly, in Γ^- simple waves α is constant throughout the region of interest. From (4.29), the Mach angle $\mathscr{A}'$ between the characteristics and $\mathbf{b}$ in the hodograph plane in the absence of gravity is given by

$$\cos^2 \mathscr{A}' = \frac{|\mathbf{b} . d\mathbf{b}|^2}{b^2 db^2} = \frac{1}{M^2}. \tag{4.32}$$

Hence $\mathscr{A}' = 90 \pm \mathscr{A}^\circ$ at points in the flow where the hodograph transformation is non-singular.

5. Examples of magnetized flows with ignorable co-ordinate z

In this section we provide sample solutions of the potential transonic equation (4.20) (with $\Phi_g = 0$) by using the hodograph transformation as described by Courant & Friedrichs (1948), von Mises (1958) and Seebass (1961). The development generalizes the solutions obtained by Seebass (1961) to include the effects of non-zero components of the velocity and magnetic field, V_z and B_z, not included in Seebass' work. For non-magnetized flows two fundamental solutions correspond to purely radial potential flow and circular flow. Other more complex flows are also possible, including the magnetized versions of spiral flows, Ringleb flows and simple waves.

In §5.1 we briefly review some aspects of the hodograph transformation for (4.18) and (4.19) in the absence of gravity. In §5.2 we use these results to consider flows in which $\mathbf{B}_p$ is purely radial in the (x, y) plane, of the form

$$\mathbf{B}_p = B_{p0} \frac{r_0}{r} \mathbf{e}_r, \tag{5.1}$$

where r denotes the radial distance from the z axis, and B_{p0} and r_0 are constants. In §5.3 we consider the analogue of azimuthal circular flows and helical flows corresponding to the solution

$$\mathbf{b} = b_0 \frac{r_0}{r} \mathbf{e}_\Theta, \tag{5.2}$$

for $\mathbf{b}$. These two fundamental solutions are combined to yield examples of spiral flows in §5.4.

5.1. *The hodograph transformation*

The essence of the hodograph transformation for the magnetized flow equations (4.18) and (4.19) (with $\Phi_g = 0$) is that the equations may be linearized by interchanging the roles of the dependent and independent variables. Hence, in the present case, writing

$$u = b_x \equiv \frac{\partial \phi}{\partial x}, \quad v = b_y \equiv \frac{\partial \phi}{\partial y}, \tag{5.3}$$

and assuming that the Jacobian $j = \partial(u,v)/\partial(x,y) \neq 0$, (4.19) and (4.18) may be rewritten as

$$x_v - y_u = 0, \tag{5.4}$$

$$(a^2-u^2)\,y_v + (a^2-v^2)\,x_u + uv(x_v+y_u) = 0, \tag{5.5}$$

where $x \equiv x(u,v)$ and $y \equiv y\,(u,v)$ are regarded as functions of u and v. The form of (5.4) suggests the introduction of a potential $\Phi(u,v)$ such that

$$x = \Phi_u, \quad y = \Phi_v, \tag{5.6}$$

which ensures that (5.4) is automatically satisfied. Using (5.6) in (5.5) now leads to the linear equation

$$(a^2-u^2)\,\Phi_{vv} + (a^2-v^2)\,\Phi_{uu} + 2uv\Phi_{uv} = 0, \tag{5.7}$$

for the potential Φ. The corresponding equation for ϕ is the transonic potential equation (4.20) with $\Phi_g = 0$, namely

$$(a^2-\phi_x^2)\,\phi_{xx} + (a^2-\phi_y^2)\,\phi_{yy} - 2\phi_x\phi_y\phi_{xy} = 0. \tag{5.8}$$

Hence the hodograph transformation described by (5.3) and (5.6) leads to a linearization of the nonlinear transonic potential flow equation (5.8). Furthermore, the transformations (5.3) and (5.6) imply that $\Phi(u,v)$ and $\phi(x,y)$ are related by the Legendre transformation

$$\Phi = ux + vy - \phi. \tag{5.9}$$

In order to fully exploit the linearization provided by the hodograph transformation, it is useful to introduce the stream function $\psi(x,y)$, where

$$\sigma u \equiv B_x = \frac{\partial \psi}{\partial y}, \quad \sigma v \equiv B_y = -\frac{\partial \psi}{\partial x}, \tag{5.10}$$

which automatically guarantees that $\nabla . \mathbf{B} = 0$. The stream function $\psi(x,y)$ is clearly equivalent to the magnetic potential $A(x,y)$ of (3.1). It also turns out to be useful to introduce the Legendre transform of $\psi(x,y)$, namely $\Psi(u,v)$, where

$$\Psi(u,v) = x\frac{\partial \psi}{\partial x} + y\frac{\partial \psi}{\partial y} - \psi \equiv -\sigma vx + \sigma uy - \psi, \tag{5.11}$$

and to develop corresponding equations for ψ and Ψ.

To obtain solutions for purely radial flow and circulatory flow, it is useful to introduce polar co-ordinates (b, θ) in the (b_x, b_y) plane, where

$$u \equiv b_x = b\cos\theta, \quad v \equiv b_y = b\sin\theta. \tag{5.12}$$

It then follows (see e.g. Courant & Friedrichs 1948) that ϕ and ψ are coupled by the equations

$$\frac{\partial \phi}{\partial \theta} = \frac{b}{\sigma}\frac{\partial \psi}{\partial b}, \tag{5.13}$$

$$\frac{\partial \phi}{\partial b} = \frac{M^2-1}{\sigma b}\frac{\partial \psi}{\partial \theta}, \tag{5.14}$$

where $M = b/a$ is the pseudo-Mach number (4.14) for magnetized flows. The integrability constraint $\phi_{b\theta}-\phi_{\theta b} = 0$ for (5.13) and (5.14) yields Chaplygin's equation

$$\frac{\partial^2 \psi}{\partial b^2}+\frac{1+M^2}{b}\frac{\partial \psi}{\partial b}+\frac{1-M^2}{b^2}\frac{\partial^2 \psi}{\partial \theta^2} = 0. \tag{5.15}$$

The characteristics of Chaplygin's equation (5.15) are given by the characteristics Γ, (4.30) and (4.31). It is also possible to obtain equations analogous to (5.13) and (5.14) linking Φ and Ψ, namely

$$\frac{\partial \Psi}{\partial \theta} = -\sigma b\frac{\partial \Phi}{\partial b}, \tag{5.16}$$

$$\frac{\partial \Psi}{\partial b} = \frac{\sigma(1-M^2)}{b}\frac{\partial \Phi}{\partial \theta}. \tag{5.17}$$

Elimination of Ψ between (5.16) and (5.17) yields the equation

$$a^2\Phi_{bb}+\frac{a^2-b^2}{b^2}(\Phi_{\theta\theta}+b\Phi_b) = 0, \tag{5.18}$$

for Φ, which is the polar co-ordinate version of (5.7). Noting that $\phi = b\Phi_b-\Phi$, (5.13), (5.14) and (5.18) yield the results

$$b\psi_b = \sigma(b\Phi_b-\Phi)_\theta, \tag{5.19}$$

$$\psi_\theta = \sigma(b\Phi_b+\Phi_{\theta\theta}), \tag{5.20}$$

relating ψ and Φ.

The Jacobian of the transformation from the (x,y) plane to the (u,v) plane is given by

$$J = \frac{\partial(x,y)}{\partial(u,v)} = \frac{1}{b^2}\left[\Phi_{bb}(\Phi_{\theta\theta}+b\Phi_b)-\left(\Phi_{b\theta}-\frac{\Phi_\theta}{b}\right)^2\right]. \tag{5.21}$$

For the hodograph method to give a single-valued solution for $u(x,y)$ and $v(x,y)$, it is necessary to restrict the solutions of (5.8) to a region where $J \neq 0$. A line along which $J = 0$ is called a limiting line; and if a limiting line is crossed then the solution may become multi-valued.

5.2. *The radial* $\mathbf{B}_p$ *solution*

The radial $\mathbf{B}_p$ solution corresponds to the solution

$$\psi = r_0\,\theta, \tag{5.22}$$

of Chaplygin's equation (5.15), where r_0 is a constant. Using the results (5.19) and (5.20) linking ψ and Φ leads to the corresponding solution

$$\Phi \equiv \Phi(b) = r_0\int^b \frac{db}{\sigma b} \tag{5.23}$$

for Φ. Equations (5.6) then yield the equations

$$x = \frac{r_0 b_x}{\sigma b^2}, \quad y = \frac{r_0 b_y}{\sigma b^2}. \tag{5.24}$$

Upon noting $\mathbf{B}_p = B_{p0}\sigma\mathbf{b}$, (5.24) yield solutions for $\mathbf{b}$ and $\mathbf{B}_p$ of the form

$$\mathbf{b} = \frac{1}{\sigma}\frac{r_0}{r}\mathbf{e}_r, \quad \mathbf{B}_p = B_{p0}\frac{r_0}{r}\mathbf{e}_r, \tag{5.25}$$

which corresponds to the solution (5.1) for $\mathbf{B}_p$.

The remaining aspects of the solution (5.1) for $\mathbf{B}_p$ follow from the energy integral (3.14) (with $\Phi_g = 0$), which may be written in the form of a potential-well equation as

$$\tfrac{1}{2}V_p^2 = E_m - U(\rho), \tag{5.26}$$

where the potential $U(\rho)$ is given by

$$U(\rho) = \tfrac{1}{2}(V_z - \Phi_E')^2 + \frac{\gamma p}{(\gamma-1)\rho}. \tag{5.27}$$

To obtain some idea of the physics implied by the potential-well equation (5.26), it is useful to introduce the dimensionless variables

$$\bar{\mathbf{V}} = \frac{\mathbf{V}}{a_{g0}}, \quad \bar{\rho} = \frac{\rho}{\rho_0}, \quad \bar{r} = \frac{r}{r_0}, \tag{5.28}$$

where $a_{g0} = (\gamma p_0/\rho_0)^{\frac{1}{2}}$, ρ_0 and r_0 denote the gas sound speed, density and radius at some canonical fixed point P_0 in the flow. The normalized form of the potential-well equation (5.26) is

$$\tfrac{1}{2}\bar{V}_p^2 = \bar{E}_m - \bar{U}(\bar{\rho}), \tag{5.29}$$

where

$$\bar{U}(\bar{\rho}) = \frac{\bar{\rho}^{\gamma-1}}{\gamma-1} + \frac{\bar{V}_{Az0}^2 M_{A0}^2 (M_{A0}^2 - 1)^2}{2(M_{A0}^2 - \bar{\rho})^2}, \tag{5.30}$$

$$\bar{E}_m = \tfrac{1}{2}M_{s0}^2 + \frac{1}{\gamma-1} + \tfrac{1}{2}\bar{V}_{Az0}^2 M_{A0}^2, \tag{5.31}$$

$$M_{s0} = \frac{V_{p0}}{a_{g0}}, \quad M_{A0} = \frac{V_{p0}}{V_{Ap0}}, \quad \bar{V}_{Az0} = \frac{V_{Az0}}{a_{g0}}. \tag{5.32}$$

Taking into account the relationship (3.6) between $\mathbf{V}_p$ and $\mathbf{B}_p$, and the solution (5.1) for $\mathbf{B}_p$, yields the expression

$$\bar{\mathbf{V}}_p = \frac{M_{s0}}{\bar{\rho}\bar{r}}\mathbf{e}_r \tag{5.33}$$

for $\bar{\mathbf{V}}_p$. Equations (5.29) and (5.33) implicitly determine the possible solutions for $\bar{\rho} = \bar{\rho}(\bar{r})$, and the other physical quantities of interest then follow in a straightforward fashion from this relationship. The expression (5.31) for $\bar{E}_m$ follows from the requirement that $\bar{\rho} = 1$ at $\bar{r} = 1$.

In some of the examples we choose P_0 (i.e. $r = r_0$) to coincide with either the fast or slow magnetosonic point, so that the magnetosonic dispersion equation

$$V_{p0}^4 - (V_{A0}^2 + a_{g0}^2)\, V_{p0}^2 + V_{Ap0}^2 a_{g0}^2 = 0 \tag{5.34}$$

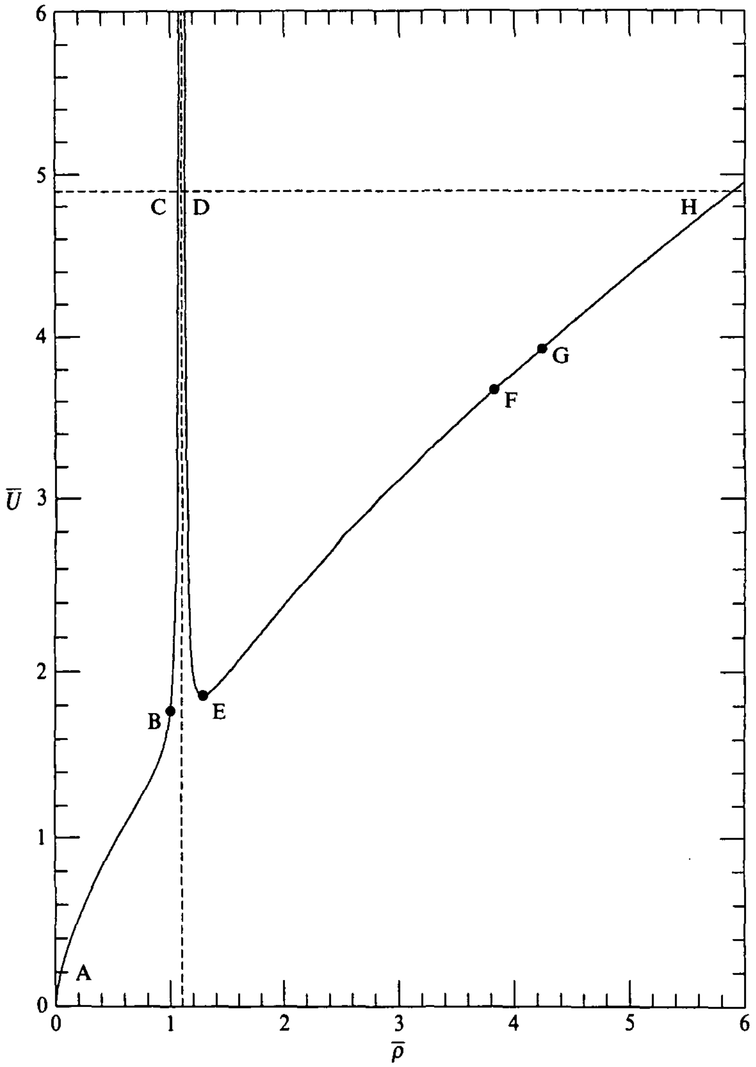

FIGURE 5. The potential $\bar{U}(\bar{\rho})$ of (5.30) versus $\bar{\rho}$ for the parameters $M_{A0} = 1{\cdot}05$, $M_{s0} = 2{\cdot}5$, $\bar{V}_{Az0} = 0{\cdot}69864$ and $\gamma = \frac{5}{3}$.

then requires that

$$\bar{V}^2_{Az0} = \frac{(M^2_{s0}-1)(M^2_{A0}-1)}{M^2_{A0}}. \tag{5.35}$$

It is of course possible that the flow does not pass through one of the magnetosonic points, in which case (5.35) cannot be satisfied. In general, $\bar{V}_{Az0}$, M_{A0} and M_{s0} are arbitrary parameters not satisfying (5.35). Hence, to obtain a solution of the normalized potential-well equation (5.27), it suffices to specify M_{A0}, M_{s0}, $\bar{V}_{Az0}$ and γ. The parameter $\bar{\Phi}'_E = \Phi'_E/a_{g0}$ needed to determine $\bar{V}_z$, (3.10), does not affect the potential-well equation (5.29), so that, without loss of physical insight, we set $\Phi'_E = 0$ in the calculations.

An example of the potential well (5.29) is displayed in figure 5, where $\bar{U}(\bar{\rho})$ is plotted as a function of $\bar{\rho}$ for the case $M_{A0} = 1{\cdot}05$, $M_{s0} = 2{\cdot}5$, $\bar{V}_{Az0} = 0{\cdot}69864$, and $\gamma = \frac{5}{3}$. From (5.35), this choice of parameters ensures that the point

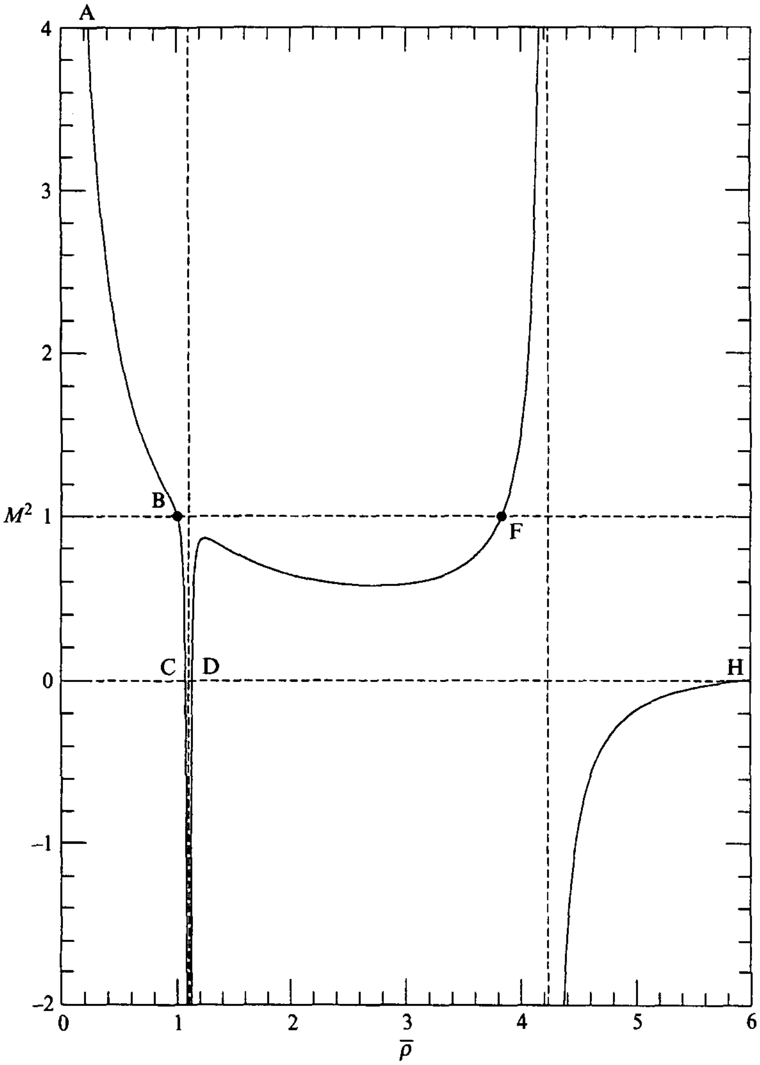

FIGURE 6. The square of the pseudo-Mach number M^2 versus $\bar{\rho}$ corresponding to the potential well of figure 5. For hyperbolic flows $M^2 > 1$, but for elliptic flows $M^2 < 1$.

$(\bar{\rho},\ \bar{r}) = (1, 1)$ corresponds to the fast magnetosonic point. For the above parameters, the energy constant $\bar{E}_m = 4{\cdot}8941$ is represented by the horizontal dashed line on the figure. The well naturally splits into a region of super-Alfvénic flow for which $0 < \bar{\rho} < M^2_{A0}$, which is represented by the curve ABC in figure 5, and a region of sub-Alfvénic flow with $\bar{\rho} > M^2_{A0}$, which is represented by the curve DEFGH. The flow speed V_p in the (x, y) plane is zero at the top of the well at the points C, D and H. From (5.26), (5.27) and (5.33), one can deduce that the points C, D and H correspond to $V_p = 0$ and $r = \infty$. The maximum flow speed V_p in the super-Alfvénic region corresponds to the point A with $\bar{\rho} = 0$ and $\bar{r} = \infty$. In the sub-Alfvénic region V_p is a maximum at the bottom of the potential well at the point E. The corresponding plot of M^2 (where M is the effective Mach number) versus $\bar{\rho}$ is displayed in figure 6. Plots of $\bar{\rho}(\bar{r})$ and $\bar{V}_p(\bar{r})$, for the super-Alfvénic flow region, obtained from (5.29), (5.30) and (5.33) are

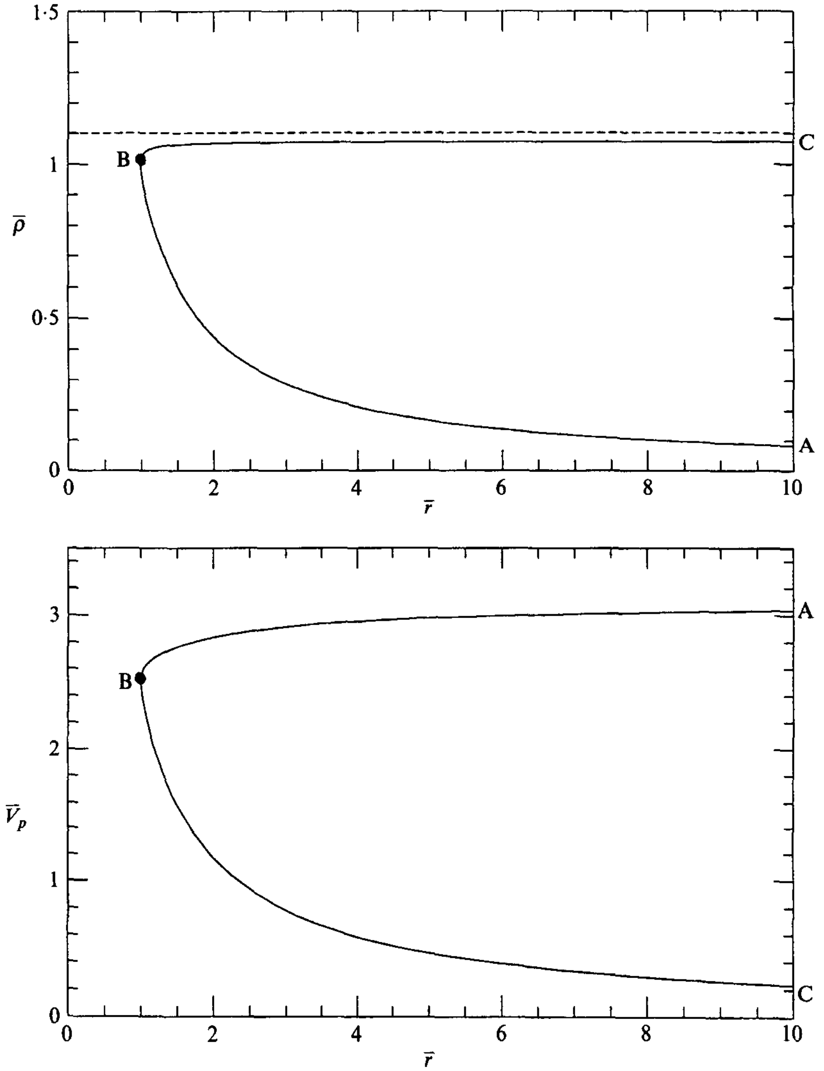

FIGURE 7. Plots of the density $\bar{\rho}$ and $\bar{V}_p$ versus $\bar{r}$ for the two super-Alfvénic 'radial' flow solutions associated with the potential well in figure 5. There are two single-valued flows, namely the super-fast flow BA, and the near-Alfvénic flow branch BC, where the point B corresponds to the fast magnetosonic point with $V_p = V_f$.

displayed in figure 7. The corresponding profiles of $\bar{\rho}(\bar{r})$ and $\bar{V}_p(\bar{r})$ for the sub-Alfvénic flow region $\bar{\rho} > M^2_{A0}$ are displayed in figure 8.

To interpret figures 5–9, it is useful to compute the derivatives $dV_p/d\rho$ and dV_p/dr by differentiating the potential-well equations (5.29), (5.30) and (5.33). We obtain

$$\frac{dV_p}{d\rho} = -\frac{(a_g^2 + V_{Az}^2)\,(V_p^2 - V_p^{*2})}{\rho V_p (V_p^2 - V_{Ap}^2)}, \tag{5.36}$$

$$\frac{dV_p}{dr} = \frac{V_p(a_g^2 + V_{Az}^2)\,(V_p^2 - V_p^{*2})}{r(V_p^2 - V_f^2)\,(V_p^2 - V_s^2)}, \tag{5.37}$$

$$\frac{d\rho}{dr} = -\frac{\rho(V_p^2 - V_{Ap}^2)\,V_p^2}{r(V_p^2 - V_f^2)\,(V_p^2 - V_s^2)}, \tag{5.38}$$

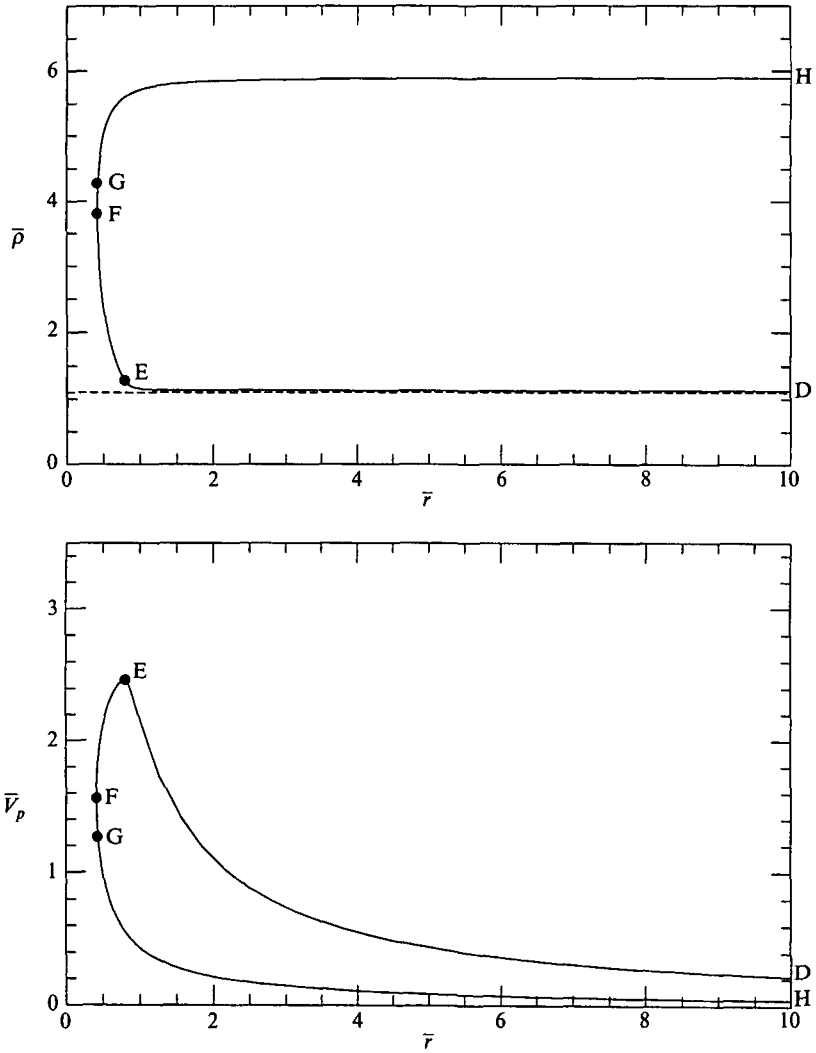

FIGURE 8. Plots of $\bar{\rho}$ and $\bar{V}_p$ versus $\bar{r}$ for the sub-Alfvénic 'radial' flow solutions corresponding to the potential well in figure 5. There are two single-valued flows starting from the slow magnetosonic point F, where $V_p = V_s$, namely FED and FGH.

where

$$V_p^{*2} = \frac{V_{Ap}^2 a_g^2}{V_{Az}^2 + a_g^2}. \tag{5.39}$$

In order to classify whether the flow is hyperbolic or elliptic, we recall from (3.30) that the Mach number M is given by

$$M^2 = 1 + \frac{(V_p^2 - V_f^2)(V_p^2 - V_s^2)}{(V_s^2 + V_f^2)(V_p^2 - V_c^2)}, \quad V_c^2 = \frac{V_{Ap}^2 a_g^2}{V_A^2 + a_g^2}. \tag{5.40}$$

For hyperbolic characteristics $M^2 > 1$, whereas for $M^2 < 1$ the flow is elliptic. The flow speeds V_f, V_{Ap}, V_s, V_p^* and V_c occurring in (5.36)–(5.40) are ordered according to

$$V_f > V_{Ap} > V_p^* > V_s > V_c. \tag{5.41}$$

The points on the potential well in figure 5 corresponding to the fast and slow magnetosonic speeds $V_p = V_f$ and $V_p = V_s$ are labelled B and F respectively;

$V_p = V_p^*$ at the point E, and $V_p = V_c$ at the point G. From figure 6, the flow is hyperbolic in the super-fast magnetosonic region $V_p > V_f > V_{Ap}$, which corresponds to the curve segment AB in figure 5. For $V_{Ap} < V_p < V_f$ (curve segment BC) the flow is elliptic. In the sub-Alfvénic flow regime the flow is hyperbolic for $V_c < V_p < V_s$, corresponding to the segment FG in figure 5, and is elliptic on the segments DEF ($V_{Ap} < V_p < V_p^*$) and GH ($0 < V_p < V_c$). On the plot of M^2 versus $\bar{\rho}$ in figure 6, $M^2 \to \infty$ as $\bar{\rho} \to \bar{\rho}_c = 4{\cdot}2333$, where $V_p = V_c$. Note from (5.40) that $M^2 < 0$ in the region $\bar{\rho} > \bar{\rho}_c$, and that $M^2 = 1$ at the fast and slow magnetosonic points B and F in figure 6.

The plots of $\bar{\rho}$ and $\bar{V}_p$ versus $\bar{r}$ for the super-Alfvénic flows in figure 7 are double-valued, and the derivatives dV_p/dr and $d\rho/dr$ diverge at the fast magnetosonic point B, where $V_p = V_f$ (see also (5.37) and (5.38)). Hence, to obtain a single-valued solution, it is necessary to restrict the flow to be either supersonic in the fast magnetosonic sense with $V_p > V_f$ (segment AB), or subsonic with $V_{Ap} < V_p < V_f$ (segment BC). One can also see the possibility of multi-valued solutions from the Jacobian (5.21) of the hodograph transformation. Using the solution (5.23) for Φ in (5.21) yields the expression

$$J = \frac{\partial(x,y)}{\partial(b_x, b_y)} = r_0^2 \left(\frac{r}{r_0}\right)^4 \frac{(M_{A0}^2 - 1)^2 (M^2 - 1)}{(M_A^2 - 1)^2} \tag{5.42}$$

for the Jacobian of the hodograph transformation. Hence $J = 0$, and limiting curves occur in the (x, y) plane at the radii $r = r_f$ and $r = r_s$ at the fast and slow magnetosonic points, where $V_p = V_f$ or $V_p = V_s$, and $M^2 = 1$. The Jacobian (5.42) diverges when $V_p = V_c$ or when $V_p = V_{Ap}$. From (5.33), the constant radial mass flux for the flows in figures 7 and 8 is given by

$$\dot{m} = 2\pi r \rho V_p = 2\pi r_0 \rho_0 V_{p0}. \tag{5.43}$$

Thus the supersonic ($V_p > V_f$) and subsonic ($V_p < V_f$) flows in figure 7 have the same mass flux and energy constant $\bar{E}_m$. The supersonic branch consists of a high-speed low-density flow, whereas the subsonic branch consists of a low-speed high-density flow.

Figure 8 illustrates the radial profiles of $\rho(r)$ and $V_p(r)$ for the sub-Alfvénic flows FED and FGH. There are two possible single-valued solutions starting from the slow magnetosonic point F, namely the low-density branch FED with $V_p^* > V_p > V_s$, and the high-density branch FGH with $0 < V_p < V_s$. The branch FED is supersonic in the slow magneto-acoustic sense, but is an elliptic flow with complex characteristics. Starting from the slow magnetosonic point F, V_p first increases until it achieves its maximum at the point E, where $V_p = V_p^*$, and then decelerates with increasing r. The main source of energy driving the flow on the segment FE is the gas enthalpy, with the density changing from $\rho = \rho_s = 3{\cdot}828$ at F to $\rho = \rho_* = 1{\cdot}2857$ at E. At larger radii $r > r_*$, beyond E, the radial flow decelerates and V_z increases at the expense of V_p (see figure 9), and the enthalpy remains roughly constant. The subsonic, slow magneto-acoustic branch FGH with $V_p < V_s$ consists of a hyperbolic section FG with $V_c < V_p < V_s$ followed by an elliptic flow regime GH at larger radii with $0 < V_p < V_c$. The kinetic flow energy $\frac{1}{2}V_p^2$ associated with the radial flow is converted to enthalpy $\gamma p/[(\gamma - 1)\rho]$ as the flow moves outward, with a relatively minor role being played by the z component of the kinetic energy $\frac{1}{2}V_z^2$.

Further features of these solutions are presented in figure 9, which displays

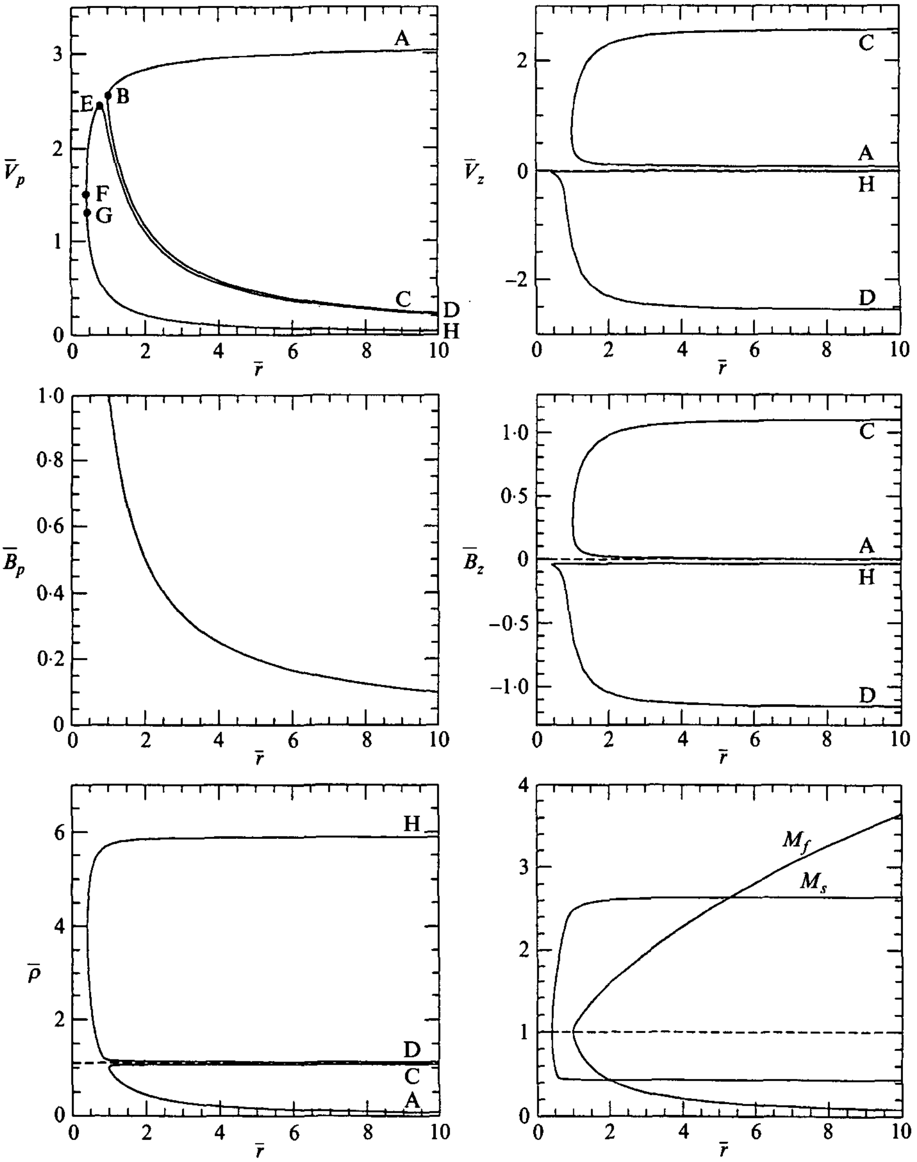

FIGURE 9. Radial profiles of $\bar{V}_p$, $\bar{B}_p$, $\bar{\rho}$, $\bar{V}_z$, $\bar{B}_z$, M_f and M_s for 'radial' flow solutions corresponding to the potential well of figure 5.

the radial variation of $\bar{V}_p$, $\bar{V}_z$, $\bar{B}_p$, $\bar{B}_z$ and $\bar{\rho}$ (note that $\bar{\mathbf{B}} = \mathbf{B}/B_{p0}$ and $\bar{\mathbf{V}} = \mathbf{V}/a_{g0}$). Also shown are the radial variation of the fast magnetosonic Mach number $M_f = V_p/V_f$ for the super-Alfvénic flow regime and the variation of the slow-mode Mach number $M_s = V_p/V_s$ for the sub-Alfvénic flow regime. The normalized forms of V_z and B_z from (3.10) and (3.11) are

$$\bar{V}_z = \Phi'_E + \bar{V}_{Az0}\frac{M_{A0}(M_{A0}^2-1)}{M_{A0}^2-\bar{\rho}}, \tag{5.44}$$

$$\bar{B}_z = \bar{V}_{Az0}\frac{M_{A0}(M_{A0}^2-1)\,\bar{\rho}}{M_{s0}(M_{A0}^2-\bar{\rho})}. \tag{5.45}$$

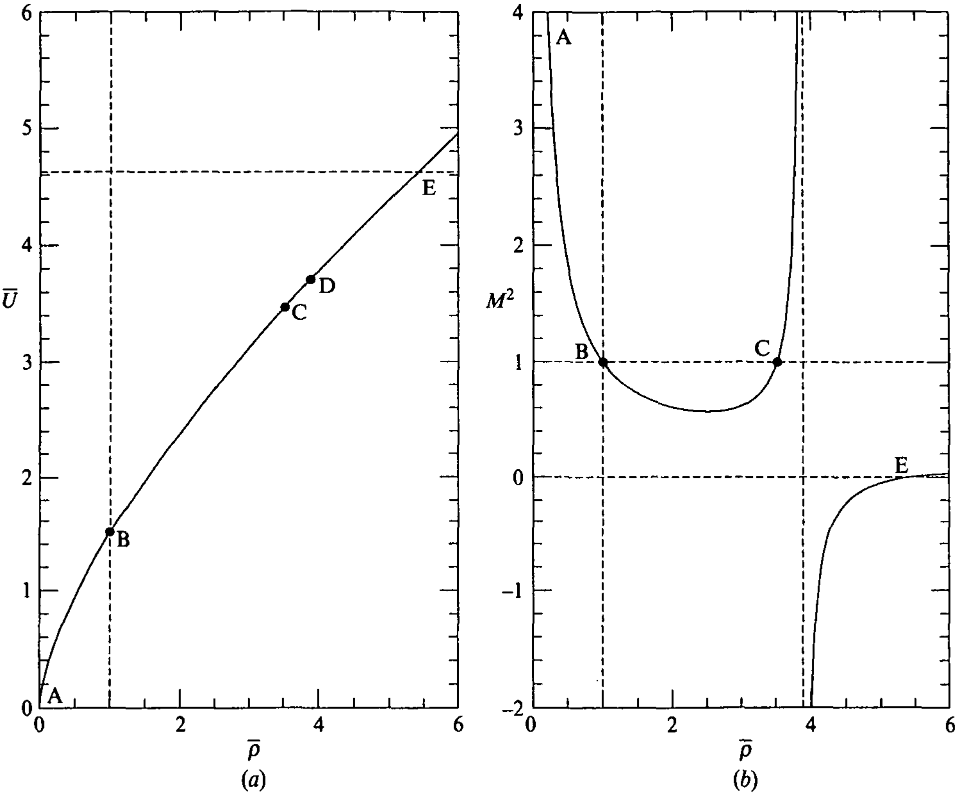

FIGURE 10. The potential well $\bar{U}(\bar{\rho})$ and the square of the pseudo-Mach number M^2 versus $\bar{\rho}$ for flows with $\bar{V}_z = \bar{B}_z = 0$, in which $M_{A0} = 1$, $M_{s0} = 2{\cdot}5$, $\bar{V}_{Az0} = 0$ and $\gamma = \frac{5}{3}$.

At sufficiently large radii $r > r_f$ ($r = r_f$ at B where $M_f = 1$) the radial flow speed profile $V_p(r)$ for the supersonic slow mode branch FED is almost identical with the subsonic fast-mode branch BC. Both the flows BC and ED are almost Alfvénic in the sense that $M_A \approx 1$ for these flows. For these solutions V_p decreases and $|V_z|$ increases with increasing r. However, $V_z > 0$ and $B_z > 0$ for the super-Alfvénic solution BC, whereas $V_z < 0$ and $B_z < 0$ for the sub-Alfvénic solution FED. The density profiles $\rho(r)$ show that the enthalpy and density variations play a more dominant role in the sluggish sub-Alfvénic flows than in the lower-density super-Alfvénic flows.

A further example of the potential-well solution (5.29) with $\Phi'_E = \bar{V}_{Az0} = 0$, $M_{A0} = 1$, $M_{s0} = 2{\cdot}5$ and $\gamma = \frac{5}{3}$ is displayed in figures 10 and 11. Since $\Phi'_E = \bar{V}_{Az0} = 0$, $\bar{V}_z = \bar{B}_z = 0$. This example corresponds to the type of solution considered by Seebass (1961) in which the fluid velocity is restricted to the (x, y) plane. Figure 10(*a*) shows the potential-well plot of $\bar{U}(\bar{\rho})$ versus $\bar{\rho}$. Unlike the potential well in figure 5, there is no singularity at the Alfvén point $\bar{\rho} = M^2_{A0} = 1$. Since $\bar{V}_{Az} = 0$, the fast magnetosonic point occurs when $V_p = V_{Ap} \equiv V_f$ at B. The slow magnetosonic point occurs at the point C, where $V_p = V_s = a_g$. At the point D the flow speed V_p matches the slow magnetosonic cusp speed (i.e. $V_p = V_c$). The solution is degenerate in the sense that two of the characteristic MHD speeds, namely the Alfvén and fast magnetosonic speeds, coincide in this example. From the plot of M^2 versus $\bar{\rho}$ in figure 10(*b*), the solution is hyperbolic in the super-Alfvénic flow regime $\bar{\rho} < M^2_{A0}$. In the sub-Alfvénic flow regime the

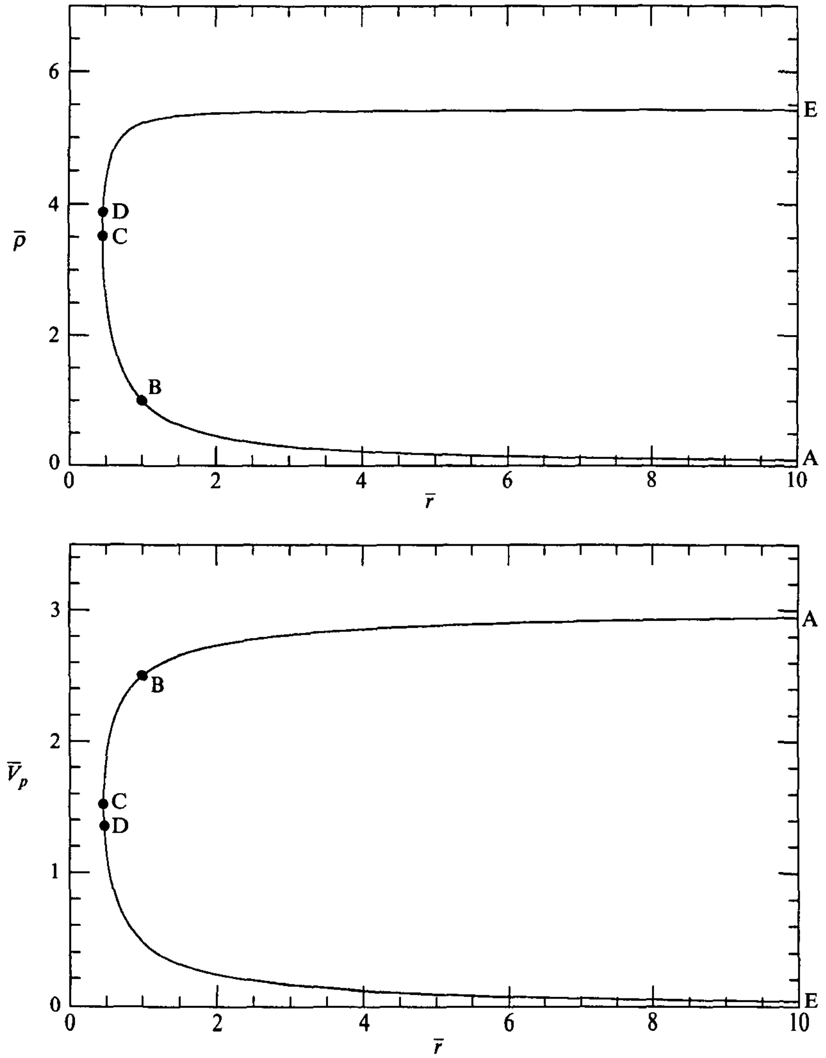

FIGURE 11. Radial profiles of $\bar\rho$ and $\bar V_p$ for the 'radial' flow solutions corresponding to the potential well in figure 10. There are two single-valued solutions starting from the gas sonic point C, where $V_p = a_g$, namely CBA and CDE.

solution is elliptic on the segment BC, where $a_g < V_p < V_{Ap}$, hyperbolic on CD, where $V_c < V_p < a_g$, and elliptic on DE, where $0 < V_p < V_c$. The plots of $\bar\rho(\bar r)$ and $\bar V_p(\bar r)$ in figure 11 show that the solutions join in a continuous fashion at the gas sonic point C. Formally, as $V_{Az0} \rightarrow 0$, one has $V_p^* \rightarrow V_{Ap}$, and (5.37) and (5.38) reduce to

$$\frac{dV_p}{dr} = \frac{V_p a_g^2}{r(V_p^2 - a_g^2)}, \tag{5.46}$$

$$\frac{d\rho}{dr} = -\frac{\rho V_p^2}{r(V_p^2 - a_g^2)}. \tag{5.47}$$

Hence $|dV_p/dr| \rightarrow \infty$ and $|d\rho/dr| \rightarrow \infty$ as $V_p \rightarrow a_g$. Thus there are two possible single-valued solutions in figure 11, namely the supersonic branch CBA with $V_p > a_g$ and the subsonic branch CDE with $V_p < a_g$. The solution CBA consists of an elliptic section CB followed by a hyperbolic flow regime BA. Similarly, the subsonic solution CDE consists of a hyperbolic flow region CD followed by an elliptic flow region DE at larger r. The near-Alfvénic flow solutions ED and BC in figure 9 do not exist for $V_{Az0} \equiv 0$.

5.3. *Helical flows*

In this section we consider the character of helical and circular flows associated with the solution (5.2) for $\mathbf{b}$. This corresponds to the solution

$$\Phi = b_0 r_0 \theta \tag{5.48}$$

of the linear equation (5.18) for Φ. Equations (5.6) then yield the solution (5.2) for $\mathbf{b}$ in the form

$$b_x = b_0 r_0 \frac{y}{r^2}, \quad b_y = -b_0 r_0 \frac{x}{r^2}, \tag{5.49}$$

which corresponds to clockwise rotation in the (x, y) plane of the vector field $\mathbf{b}$ if $b_0 r_0 > 0$. The corresponding solution for the stream function ψ may be determined from (5.19) and (5.20) as

$$\psi = -b_0 r_0 \int \sigma \frac{db}{b}, \tag{5.50}$$

where σ is the pseudo-fluid density (4.5).

Taking $b_0 = -1$, (5.2) and (4.5) yield the solutions

$$\mathbf{b} = \frac{r_0}{r}\mathbf{e}_\Theta, \quad \mathbf{B}_p = B_{p0}\frac{M_{A0}^2 - 1}{M_A^2 - 1}\frac{r_0}{r}\mathbf{e}_\Theta, \tag{5.51}$$

for $\mathbf{b}$ and $\mathbf{B}_p$, where $\mathbf{e}_\Theta$ is the azimuthal unit vector in the (x, y) plane. The remaining aspects of the solution then follow from the potential-well equations (5.26)–(5.32) used in the discussions of the purely radial flow solution in §5.2. Since the normalized magnetic field component $\bar{B}_p = \bar{B}_\Theta$ in the (x, y) plane is related to the corresponding velocity component $\bar{V}_p \equiv \bar{V}_\Theta$ by the equation

$$\bar{B}_\Theta \equiv \bar{B}_p = \frac{\bar{\rho}\bar{V}_p}{M_{s0}} \tag{5.52}$$

(see (3.6)), we may identify the behaviour of the azimuthal field with that of the azimuthal mass flux. Equations (5.51) and (5.52) and the potential-well equation (5.29) implicitly yield the dependence of the density ρ on the cylindrical radius r via the equation

$$\bar{r}^2 = \frac{M_{s0}^2 (M_{A0}^2 - 1)^2}{2(M_{A0}^2 - \bar{\rho})^2 [\bar{E}_m - \bar{U}(\bar{\rho})]}. \tag{5.53}$$

The components of $\mathbf{V}$ and $\mathbf{B}$ along the z axis follow from (5.44) and (5.45).

Figure 12 illustrates an example of a helical-flow solution for the case $M_{A0} = 1{\cdot}1$, $M_{s0} = 2{\cdot}0$, $\gamma = \frac{5}{3}$ and $\bar{V}_{Az0} = 0{\cdot}721\,57$, where the value of $\bar{V}_{Az0}$ is determined by the normalization equation (5.35). The figure shows plots of the velocity field components $\bar{V}_\Theta$ and $\bar{V}_z$, the magnetic field components $\bar{B}_\Theta$ and $\bar{B}_z$, the density $\bar{\rho}$, and the fast and slow magnetosonic Mach numbers M_f and M_s as

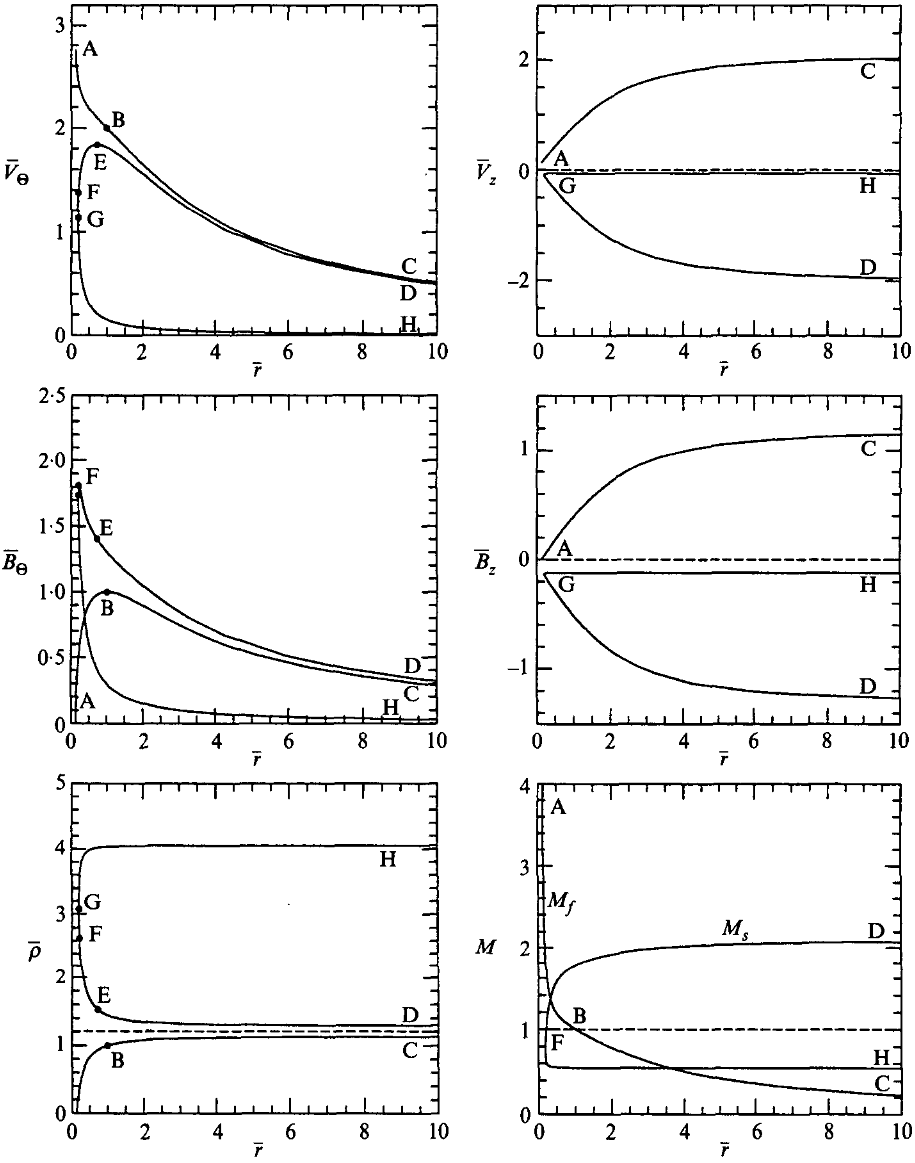

FIGURE 12. Radial profiles of $\bar V_\Theta$, $\bar B_\Theta$, $\bar \rho$, $\bar V_z$, $\bar B_z$, M_f and M_s for helical flow solutions with $M_{A0} = 1{\cdot}1$, $M_{s0} = 2{\cdot}0$, $\bar V_{Az0} = 0{\cdot}721\,57$ and $\gamma = \frac{5}{3}$.

functions of $\bar r$. The points A, B and C on the super-Alfvénic flow solution ($V_p > V_{Ap}$) and the points D, E, F, G and H on the sub-Alfvénic flow branch have the same physical meaning as in the potential-well diagram illustrated in figure 5. Hence C, D and H signify the points at $\bar r = \infty$, where $\bar V_p \rightarrow 0$, and correspond to the top of the potential well. The points B and F correspond to points in the flow where the azimuthal flow velocity V_Θ matches the fast and slow magnetosonic speeds V_f and V_s respectively. On the sub-Alfvénic branch $V_p = V_p^*$ at E and $V_p = V_c$ at G. As in the radial flow solution examples, the flow is hyperbolic in the super-Alfvénic flow regime AB, where $V_p > V_f$, and for the slow-mode regime FG, where $V_c < V_p < V_s$, but is otherwise elliptic.

To obtain some physical insight into the character of the solutions, it is useful to note that the momentum equation (2.2) for this class of flows reduces to the radial momentum equation

$$-\rho\frac{V_\Theta^2}{r} = -\frac{dp}{dr} - \frac{d}{dr}\left(\frac{B_z^2+B_\Theta^2}{2\mu}\right) - \frac{B_\Theta^2}{\mu r}. \tag{5.54}$$

Hence the centripetal force on the fluid, $-\rho V_\Theta^2/r$, is balanced by the gas and magnetic pressure gradients and the magnetic tension force, $-B_\Theta^2/\mu r$. The balance between the different force components in (5.54) is significantly different in the different flow regimes. Thus, for example, in the elliptic flow regime $0 < V_p < V_c$ (GH) the gas pressure gradient, $-dp/dr$, and the magnetic tension forces, $-B_\Theta^2/\mu r$, are inwards, but the magnetic pressure gradient force, $-d[(B_\Theta^2+B_z^2)/2\mu]/dr$, is outwards. On the other hand, for the supersonic fast-mode flow regime $V_p > V_f$ (AB) all the forces on the fluid element are inwards.

Further aspects of the solution may be assessed from the radial derivatives

$$\frac{dB_p}{dr} = \frac{B_p}{r}\frac{(V_p^2-V_f^2)(V_p^2-V_s^2)}{(V_A^2+a_g^2)(V_p^2-V_c^2)}, \tag{5.55}$$

$$\frac{d\rho}{dr} = \frac{\rho}{r}\frac{V_p^2(V_p^2-V_{Ap}^2)}{(V_A^2+a_g^2)(V_p^2-V_c^2)}, \tag{5.56}$$

$$\frac{dV_p}{dr} = -\frac{V_p}{r}\frac{(a_g^2+V_{Az}^2)(V_p^2-V_p^{*2})}{(V_A^2+a_g^2)(V_p^2-V_c^2)}. \tag{5.57}$$

Hence $B_p \equiv B_\Theta$ and the azimuthal mass flux ρV_Θ (see (5.52)) have maxima when the azimuthal flow speed V_p matches either the fast or slow magnetosonic speeds V_f or V_s at the points B and F; V_p is maximum in the slow-mode regime at the point E, where $V_p = V_p^*$. Each of the derivatives in (5.55)–(5.57) diverges at the point G, where $V_p = V_c$.

The maximum azimuthal speed for these flows occurs on the fast-mode branch at the point A, where cavitation occurs (i.e. $\rho \to 0$), at a radius $r = r_{\min}$, which is the value of r at $\rho = 0$ given by (5.53). The flow is restricted to the region $r > r_{\min}$. The V_z velocity component at $r = r_{\min}$ is non-zero, and is determined by setting $\bar{\rho} = 0$ in (5.44) (note that $\Phi_E' = 0$ is assumed in figure 12). The azimuthal flow speed V_Θ decreases monotonically and V_z increases with increasing radius on the fast-mode branch ABC. The velocity $\mathbf{V} \to V_z \mathbf{e}_z$ as $r \to \infty$, so that the flow is essentially non-rotating at large radii.

5.4. *Spiral flows*

Solutions for spiral flows can be obtained by linear superposition of the potentials Φ corresponding to radial, (5.23), and circular, (5.48), flows. The resulting potential Φ is of the form

$$\Phi = r_0\left[(\cos\alpha_0)\int\frac{db}{\sigma b} - (\sin\alpha_0)\,\theta\right], \tag{5.58}$$

where the first term on the right-hand side represents purely radial flow, and the θ-dependent term represents circular flow. Since (5.18) for Φ is linear, a linear superposition of independent solutions is again a solution. The corresponding stream function ψ is readily determined from (5.19) and (5.20) as

$$\psi = r_0\left[(\sin\alpha_0)\int\frac{db}{\sigma b}+(\cos\alpha_0)\,\theta\right]. \tag{5.59}$$

From (5.6) and (5.58), we find

$$x = \frac{r_0}{b^2}\left[(\sin\alpha_0)\,b_y+(\cos\alpha_0)\frac{b_x}{\sigma}\right],$$

$$y = \frac{r_0}{b^2}\left[-(\sin\alpha_0)\,b_x+(\cos\alpha_0)\frac{b_y}{\sigma}\right]. \tag{5.60}$$

Equations (5.60) are readily inverted to yield

$$b_x = \frac{r_0}{r^2}\left[(\cos\alpha_0)\frac{x}{\sigma}-(\sin\alpha_0)\,y\right],$$

$$b_y = \frac{r_0}{r^2}\left[(\sin\alpha_0)\,x+(\cos\alpha_0)\frac{y}{\sigma}\right], \tag{5.61}$$

where $r^2 = x^2+y^2$. Alternatively, using polar co-ordinates $(x,y) = r(\cos\Theta, \sin\Theta)$, (5.61) give the solution

$$\mathbf{b} = \frac{\cos\alpha_0}{\sigma\bar{r}}\mathbf{e}_r+\frac{\sin\alpha_0}{\bar{r}}\mathbf{e}_\Theta \tag{5.62}$$

for $\mathbf{b}$, where $\bar{r} = r/r_0$ is the normalized form of r.

Having established the solution (5.62) for $\mathbf{b}$, (4.5) and (5.45) give the solution for $\bar{\mathbf{B}} = \mathbf{B}/B_{p0}$ in the form

$$\bar{\mathbf{B}} = \frac{\bar{B}_{r0}}{\bar{r}}\mathbf{e}_r+\bar{B}_{\Theta_0}\frac{(M_{A0}^2-1)\,\bar{\rho}}{(M_{A0}^2-\bar{\rho})\,\bar{r}}\mathbf{e}_\Theta+\frac{\bar{V}_{Az0}M_{A0}(M_{A0}^2-1)\,\bar{\rho}}{M_{s0}(M_{A0}^2-\bar{\rho})}\mathbf{e}_z, \tag{5.63}$$

where

$$(\bar{B}_{r0},\bar{B}_{\Theta0}) = (\cos\alpha_0, \sin\alpha_0) \tag{5.64}$$

are the normalized components of $\mathbf{B}_p$ at the canonical radius $r = r_0$. The corresponding normalized velocity field $\bar{\mathbf{V}} = \mathbf{V}/a_{g0}$ for the case $\Phi'_E = 0$ is parallel to $\mathbf{B}$, and is given by

$$\bar{\mathbf{V}} = M_{s0}\frac{\bar{\mathbf{B}}}{\bar{\rho}}. \tag{5.65}$$

As in §5.2, we choose the radius $r = r_0$ to coincide with the fast magnetosonic point, so that $\bar{V}_{Az0}$ is determined from (5.35). The polar co-ordinate form of the transformations (5.61), with $\mathbf{b} = b(\cos\theta, \sin\theta)$ yields the equivalent transformations

$$\Theta = \theta-\tan^{-1}(\sigma\tan\alpha_0), \tag{5.66}$$

$$\bar{r}^2b^2 = \sin^2\alpha_0+\frac{\cos^2\alpha_0}{\sigma^2}. \tag{5.67}$$

Since $\sigma = 1$ at $r = r_0$, (5.66) yields

$$\alpha_0 = \theta_0-\Theta_0, \tag{5.68}$$

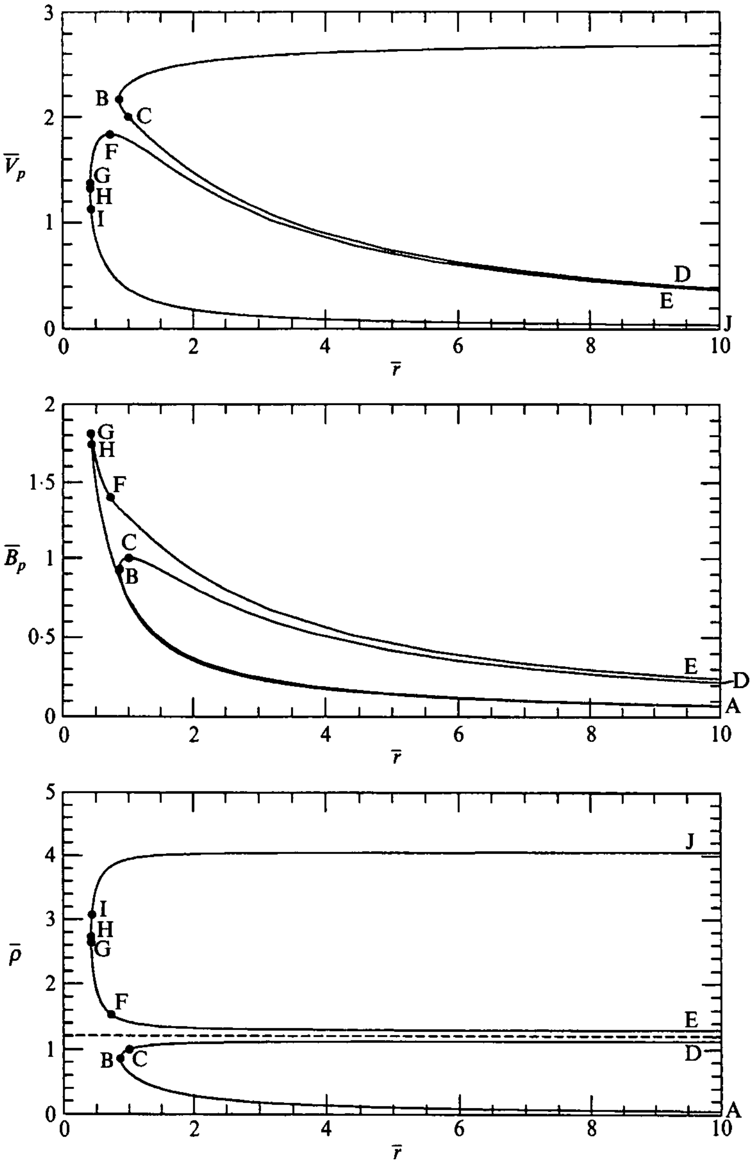

FIGURE 13. Radial profiles of $\bar V_p$, $\bar B_p$ and $\bar\rho$ for spiral flow solutions with $M_{A0} = 1\cdot1$, $M_{s0} = 2\cdot0$, $\bar V_{Az0} = 0\cdot72157$ and $\gamma = \frac{5}{3}$. The profiles have vertical tangents at the limit lines at the points B and H, where the radial flow speed $V_r = c$, with c being the appropriate magneto-acoustic phase speed on the Mach cone.

so that α_0 may be identified as the angle between $\mathbf{B}_p$ and the radial direction at $r = r_0$.

The remaining equation needed to determine the solution is the energy equation (5.29). From (5.29) and (5.65), the dependence of the density $\bar\rho$ on radius $\bar r$ is determined implicitly from the potential-well equation in the form

$$\bar r^2 = \frac{M_{s0}^2\,[\bar B_{r0}^2 + \bar B_{\Theta_0}^2(M_{A0}^2-1)^2\,\bar\rho^2/(M_{A0}^2-\bar\rho)^2]}{2\bar\rho^2\,[\bar E_m - \bar U(\bar\rho)]}. \tag{5.69}$$

The resulting solutions for ρ, $\mathbf{V}$ and $\mathbf{B}$ depend only on radial distance $\bar{r}$ from the z axis.

The streamlines of the flow,

$$\frac{dr}{V_r} = \frac{r\,d\Theta}{V_\Theta} = \frac{dz}{V_z}, \tag{5.70}$$

using the solution (5.65) for $\mathbf{V}$ may be integrated to yield

$$\Theta - \Theta_0 = (\tan\alpha_0)\int_{r_0}^{r} \sigma\frac{dr}{r}, \tag{5.71}$$

$$\bar{z} - \bar{z}_0 = \frac{\bar{V}_{Az0}M_{A0}}{M_{s0}\cos\alpha_0}\int_{\bar{r}_0}^{\bar{r}} \sigma\bar{r}\,d\bar{r}. \tag{5.72}$$

The projection of the streamlines (5.71) on the (x, y) plane is of course equivalent to the equation $\psi = \text{const}$, where ψ is the stream function (5.59) – a result that may be verified from the transformations (5.66) and (5.67).

Examples of the spiral flow solution (5.62)–(5.69) for the parameter values $M_{A0} = 1{\cdot}1$, $M_{s0} = 2$, $\bar{V}_{Az0} = 0{\cdot}72157$, and $\alpha_0 = 45°$ are given in figures 13 and 14. Figure 13 shows the dependence of $\bar{V}_p$, $\bar{B}_p$ and $\bar{\rho}$ on radial distance $\bar{r}$ from the z axis, whereas figure 14 shows the variations of the magnetic and velocity vector field components (B_r, B_Θ, B_z) and (V_r, V_Θ, V_z). To interpret figures 13 and 14, it is useful to determine the derivatives $d\rho/dr$, dV_p/dr and dB_p/dr from (5.63)–(5.65) as

$$\frac{d\rho}{dr} = -\frac{\rho(V_p^2 - V_{Ap}^2)\,V_p^2}{rD}, \tag{5.73}$$

$$\frac{dV_p}{dr} = \frac{V_p(a_g^2 + V_{Az}^2)\,(V_p^2 - V_p^{*2})}{rD}, \tag{5.74}$$

$$\frac{dB_p}{dr} = -\frac{B_p(V_p^2 - V_f^2)\,(V_p^2 - V_s^2)}{rD}, \tag{5.75}$$

where

$$D = \Delta - V_\Theta^2 V_p^2, \quad \Delta = (V_p^2 - V_f^2)\,(V_p^2 - V_s^2). \tag{5.76}$$

In (5.73)–(5.76), V_f and V_s denote the fast and slow magnetosonic speeds (3.23), and V_p^* is defined in (5.39).

To obtain some physical insight into the singularity $D = 0$, in (5.73)–(5.75) it is useful to note from the Mach cone analysis of §3, that the Mach number M of the flow from (3.29) and (3.52) is given by the formulae

$$M^2 = \frac{V_p^2}{c^2} = \frac{V_p^4}{V_p^4 - \Delta}, \tag{5.77}$$

where c denotes the appropriate magnetosonic phase speed measured on the Mach cone. From (5.76) and (5.77), we find

$$\Delta = V_p^2(V_p^2 - c^2), \quad D = V_p^2(V_r^2 - c^2). \tag{5.78}$$

Hence the radial derivative $|d\rho/dr| \to \infty$ and $D \to 0$ when the radial flow speed V_r matches the magnetosonic phase speed c on the Mach cone. At this point in the flow the characteristic equations (3.31) reduce to

$$V_p^2\,\xi_r\left[(V_\Theta^2 - V_r^2)\,\xi_r - 2\frac{V_\Theta V_r}{r}\xi_\Theta\right] = 0. \tag{5.79}$$

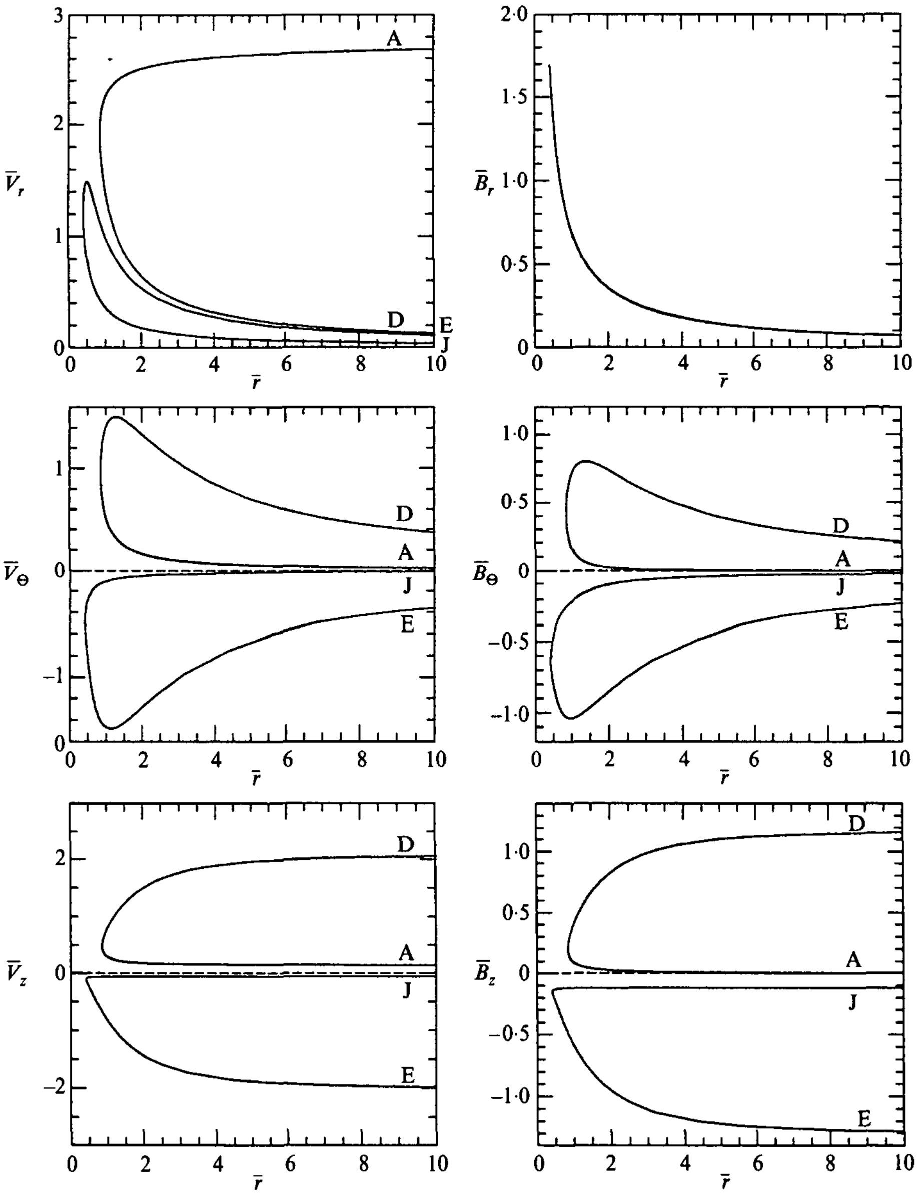

FIGURE 14. Radial profiles of the velocity field components (V_r, V_Θ, V_z) and magnetic field components (B_r, B_Θ, B_z) for spiral flow solutions with the same parameters as figure 13.

One of the solutions of (5.79), namely $\xi_r = 0$, shows that locally at the radial sonic point, where $D = 0$ and $V_r^2 = c^2$, this characteristic is purely azimuthal (i.e. $\xi = \Theta$ at this point) and the **k** vector of the magnetosonic wave of interest is purely radial. In terms of the pseudo-fluid velocity **b** and sound speed a, one can obtain equivalent formulae for Δ and D, namely

$$\Delta = \frac{V_p^4(b^2 - a^2)}{b^2}, \quad D = \frac{V_p^4(b_r^2 - a^2)}{b^2}. \tag{5.80}$$

Hence at the radial sonic point $D = 0$ and $b_r^2 = a^2$.

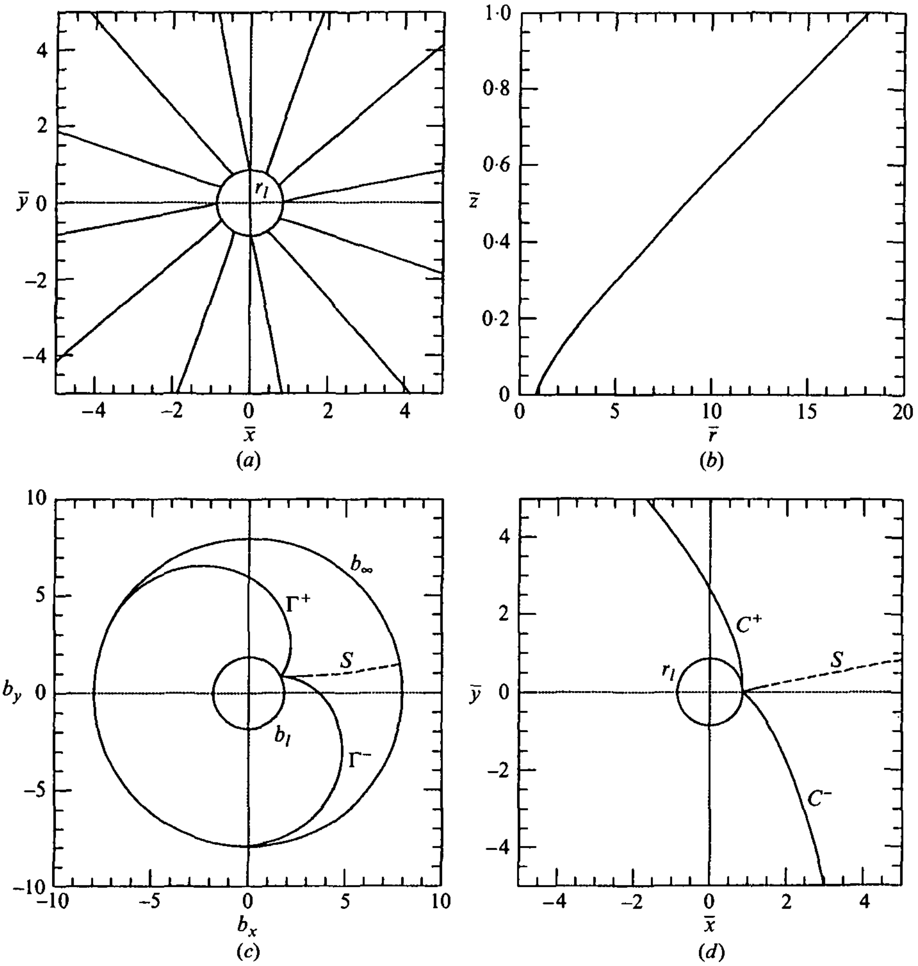

FIGURE 15. Examples of streamline projections on (*a*) the (x, y) plane and (*b*) the (z, r) plane corresponding to the super-Alfvénic spiral flow solution BA of figure 13. (*c*) shows the characteristics Γ^+ and Γ^- in the (b_x, b_y) hodograph plane, and the streamline S that meets the characteristics on the limit circle at $b = b_l$. (*d*) shows the corresponding characteristics C^+ and C^- and streamline S in the (x, y) plane.

It is evident from figure 13 that at the points B and H, where $V_r^2 = c^2$ and $D = 0$, the fast and slow magnetosonic solutions become double-valued. This fact is related to the vanishing of the Jacobian (5.21):

$$J = \frac{\partial(x, y)}{\partial(b_x, b_y)} = \frac{r^2(b_r^2 - a^2)}{a^2 b^2} \equiv \frac{r^2(\Delta - V_p^2 V_\Theta^2)}{b^2(V_A^2 + a_g^2)(V_p^2 - V_c^2)} \tag{5.81}$$

at the radial sonic point, corresponding to a limiting line in the hodograph transformation. The Jacobian (5.81) diverges as $V_p \rightarrow V_c$, where $c \rightarrow 0$ and $M^2 \rightarrow \infty$.

5.4.1. *Streamlines and characteristics for spiral flows*

Although the results of figure 14 contain the basic information on the variation of **V** and **B** for the spiral flow, a more vivid characterization of the flow is obtained from the flow streamlines (5.71) and (5.72) and from the

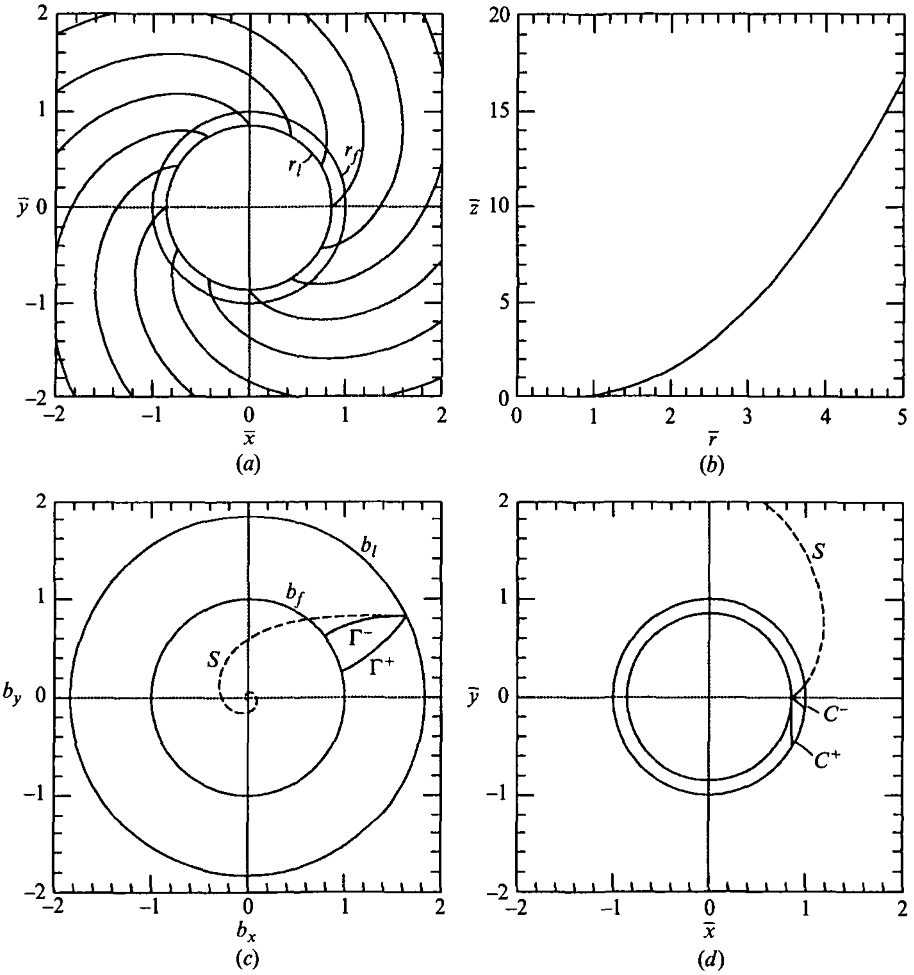

FIGURE 16. Same as figure 15, except for the near-Alfvénic spiral flow branch BCD of figure 13. The circles $b = b_l$ and $b = b_f$ correspond to the limit circle and fast magnetosonic point respectively.

hodograph plane characteristics Γ^+ and Γ^- described by (4.30) and (4.31). The streamlines (5.71) and (5.72) and the characteristics (4.30) and (4.31) are most simply evaluated by converting the integrals involved to integrals over the density $\bar{\rho}$.

The streamlines and characteristics for the fast magnetosonic spiral flow BA of figure 13 (obtained by numerical integration) are displayed in figure 15. Figures 15(*a*) and (*b*) show the streamline projections on the (x, y) and (z, r) planes. Figure 15(*a*) shows that the spiral flow branch BA is almost a radial flow, with the circle at radius $r = r_l$ representing the limit line (i.e. the point B in figure 13).

Examples of the characteristics Γ^+ and Γ^- in the (b_x, b_y) hodograph plane are shown in figure 15(c). The circles at $b = b_l$ and $b = b_\infty$ correspond to the limit line $r = r_l$ and $r = \infty$ respectively. The dashed curve S represents a fluid streamline in the hodograph plane. The constants in the integrals (5.71), (5.72) and (4.30), (4.31) have been chosen so that the streamline S and the characteristics

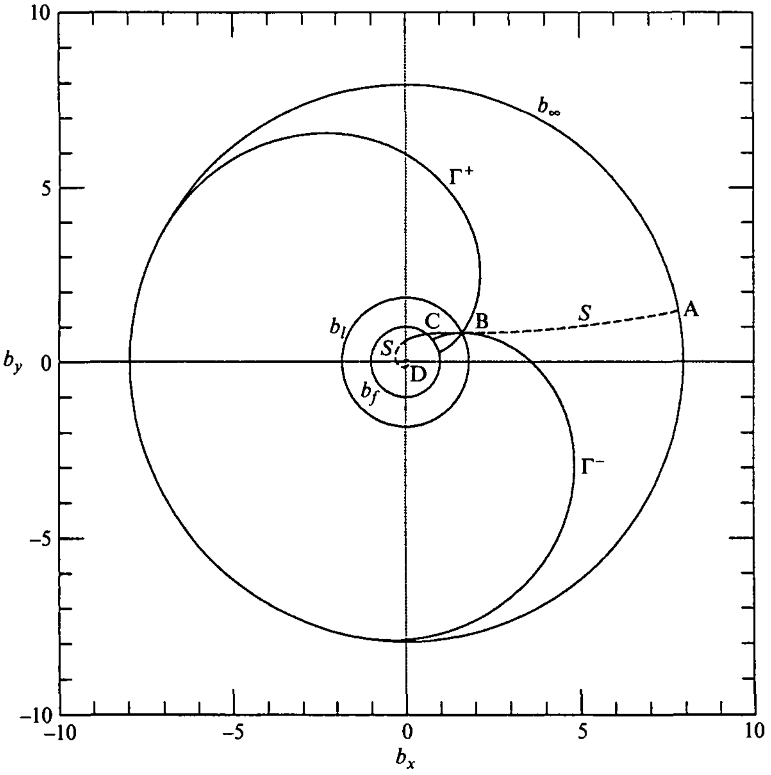

FIGURE 17. A unified view of the characteristics and streamlines S of figures 15 and 16 in the hodograph plane. The flow BA lies outside the limit circle $b = b_l$, whereas the flow BCD lies inside the limit circle.

meet at the limit circle $b = b_l$. By varying the integration constants, the hyperbolic flow region $b_l < b < b_\infty$ can be covered by a net of characteristics Γ^+ and Γ^-. The behaviour of the flow streamlines and characteristics is complicated in the immediate vicinity of the limit line, where the hodograph transformation is singular. A discussion of the character of the hodograph map and characteristics in the vicinity of the limit line for the case of pure gas dynamics is given by Courant & Friedrichs (1948, chap. 2, §30). The characteristics Γ^+ and Γ^- in figure 15(*c*) are visually similar to the epicycloid characteristics for gasdynamics discussed by Courant & Friedrichs (1948, chap. 4). The corresponding characteristics C^+ and C^- and streamline S in the (x, y) plane are displayed in figure 15(*d*). Note that the characteristic C^+ is tangent to the limit circle at $r = r_l$.

The second possible solution for super-Alfvénic flow in figure 13 is the solution branch BCD. The point B corresponds to the limit line where $V_r = c$, and the point C represents the fast magnetosonic point where $V_p = V_f$. The projections of the streamlines on the (x, y) and (z, r) planes for this spiral flow are shown in figures 16(*a*) and (*b*). Unlike the flow in figure 15, this near-Alfvénic flow has a pronounced spiral structure. The flow is hyperbolic between the two circles $r = r_l$ (the limit line) and $r = r_f$ (the fast magnetosonic point). Figure 16(*c*) shows the characteristics Γ^+ and Γ^- and the streamline S, which meet at the limit circle $b = b_l$. The inner circle $b = b_f$ represents the fast

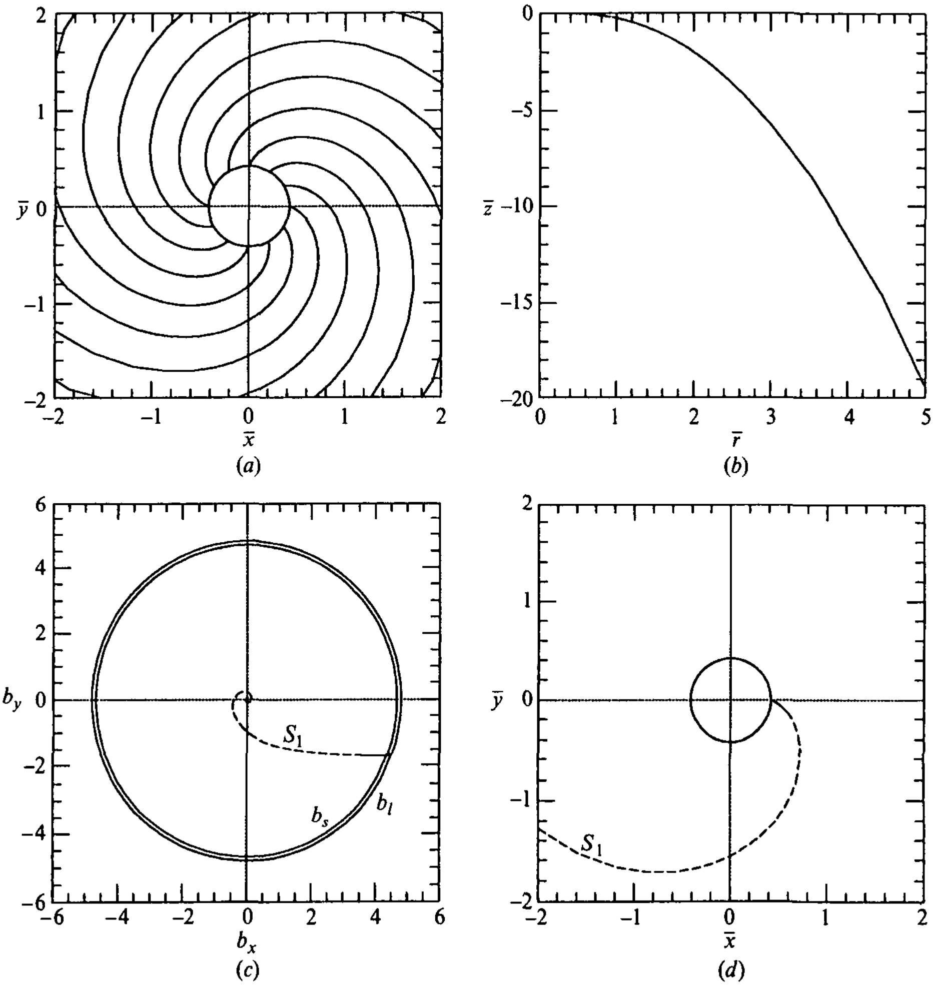

FIGURE 18. Streamlines and characteristics for the sub-Alfvénic spiral flow HGFE of figure 13. The flow is hyperbolic for $b_s < b < b_l$ in (c).

magnetosonic point. The characteristics C^+ and C^- in the (x, y) plane are shown in figure 16(d), in which the characteristic C^+ is tangent to the limit circle $r = r_l$. A unified view of the two super-Alfvénic spiral flow solutions is presented in figure 17, which shows the characteristics Γ^+ and Γ^- and the spiral flow streamlines S in the hodograph plane for the flows BA and BCD depicted in figures 15 and 16. The points A and D correspond to $r = \infty$, and the two single-valued flows extend from the limit line $b = b_l$.

Figures 18 and 19 show respectively the sub-Alfvénic solutions HGFE and HIJ in figure 13. The main point to note is that the spirals rotate in the opposite sense to the super-Alfvénic spirals in figures 15 and 16, and V_z and B_z are along the negative z axis. In order to resolve the structure of the streamlines and characteristics, figure 20 shows an expanded view of the hyperbolic flow region in the hodograph plane. The curves labelled $b = b_s$, $b = b_l$ and $b = b_c$ represent the slow magnetosonic circle ($V_p = V_s$), the limit circle ($V_r = c$) and the slow magnetosonic cusp circle ($V_p = V_c$) respectively. The streamlines S_1 and S_2

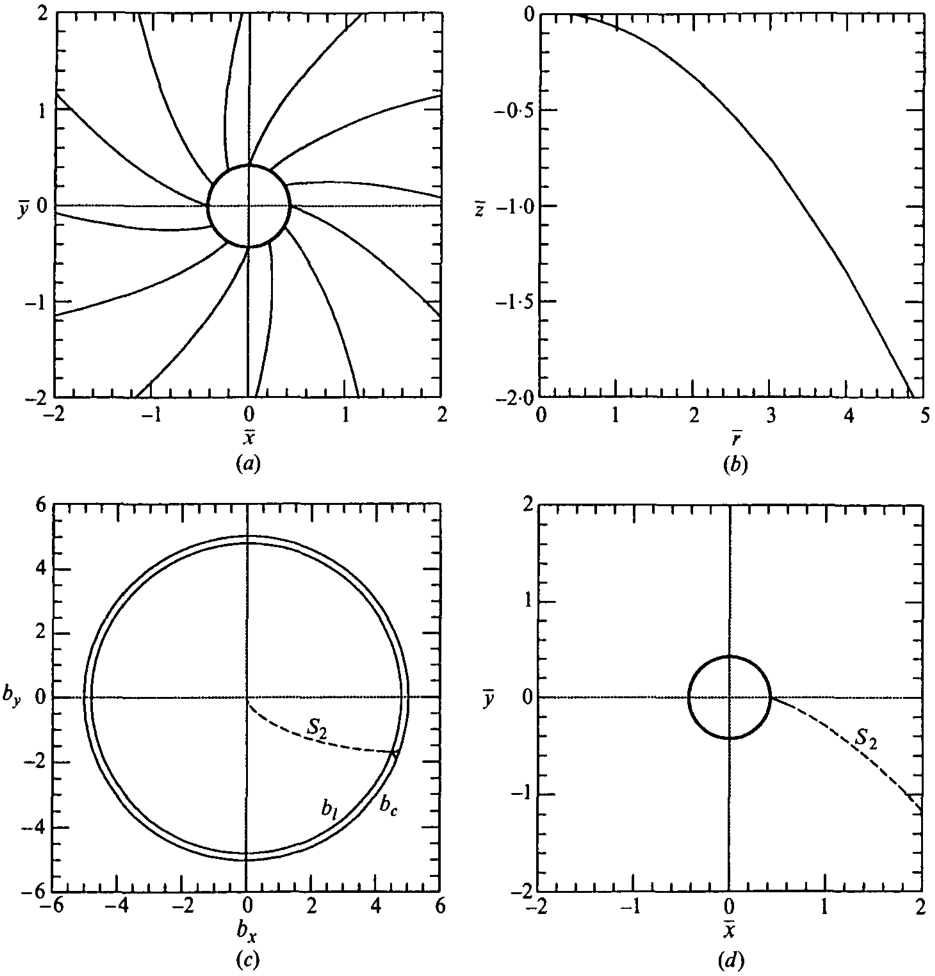

FIGURE 19. Same as figure 18, except for the sub-Alfvénic spiral flow solution HIJ of figure 13. The flow is hyperbolic for b in the range $b_l < b < b_c$ in figure (*c*).

associated with the flow in figure 18 are tangent to the characteristic Γ^+ at the limit circle.

6. Flows with an ignorable azimuthal co-ordinate ϕ

In this section we indicate the extension of the results of §§3 and 4 to the case of steady MHD flows with an ignorable co-ordinate ϕ of a spherical polar co-ordinate system (r, θ, ϕ). The corresponding version of the generalized Grad–Shafranov equation, or trans-field equation, analogous to (3.15) has been used extensively in modelling magnetized wind flows and jets (see e.g. Heinemann & Olbert 1978; Tsinganos 1981; Sakurai 1985, 1990; Camenzind 1986, 1987; Hu & Low 1989; Heyvaerts & Norman 1989). We first outline the derivation of the trans-field equation for the above geometry, and then determine under what conditions the trans-field equation coupled with Gauss' law $\nabla . \mathbf{B} = 0$, leads to the potential transonic flow equation. We remark that the conditions for the potential transonic flow to apply are sufficiently stringent

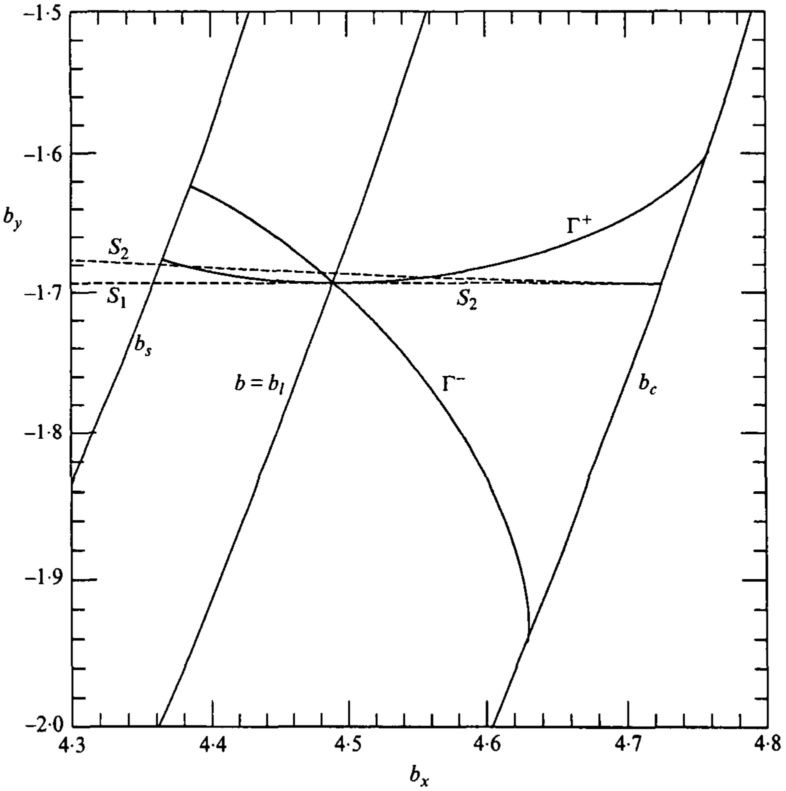

FIGURE 20. Expanded view of the characteristics Γ^+ and Γ^- for the spiral flows of figures 18(*c*) and 19(*c*). The curves $b = b_s$, $b = b_l$ and $b = b_c$ are segments of circles in the hodograph plane corresponding to the slow magnetosonic point, the slow-mode limit circle and the magnetosonic cusp point where $V_p = V_c$. S_1 and S_2 are the streamlines of figures 18(*c*) and 19(*c*), which both issue forth from the limit line.

that it is not possible to satisfy the usual regularity conditions applied in wind theory at the Alfvén critical surface. Hence this approach will not be of any use for models of winds near the Alfvén surface, but could be of use for sub-Alfvénic siphon flows in the solar atmosphere, or for subsonic and supersonic flows past a stationary object (e.g. the magnetosphere of a planet). Solutions of the potential transonic equation should also be of use in describing the collimation of radio jets by the Lorentz force.

6.1. *The trans-field equation*

Since ϕ is an ignorable co-ordinate, Gauss' law $\nabla . \mathbf{B} = 0$ and the continuity equation (2.1) imply that $\mathbf{B}$ and $\mathbf{V}$ may be expressed in the form

$$\mathbf{B} = \nabla \times \left(\frac{A}{r \sin\theta}\mathbf{e}_\phi\right) + B_\phi(r,\theta)\,\mathbf{e}_\phi = \mathbf{B}_p + B_\phi \mathbf{e}_\phi, \tag{6.1}$$

$$\mathbf{V} = \frac{1}{\mu\rho}\nabla \times \left(\frac{\psi}{r \sin\theta}\mathbf{e}_\phi\right) + V_\phi \mathbf{e}_\phi = \mathbf{V}_p + V_\phi \mathbf{e}_\phi. \tag{6.2}$$

The projection of the magnetic field on the (r,θ) plane is given by the contours of $A(r,\theta) = \text{const}$, whereas $\psi(r,\theta) = \text{const}$ gives the projection of the fluid streamlines. It is of interest to note that $\mathbf{B}_p = \nabla \times (A \nabla\phi) = \nabla A \times \nabla\phi$.

The ϕ component of Faraday's law in the form $\mathbf{E} = -\mathbf{V}\times\mathbf{B} = -\nabla\Phi_E(r,\theta)$ gives

$$E_\phi = -\frac{1}{\mu\rho r^3\sin^2\theta}\frac{\partial(\psi,A)}{\partial(r,\theta)} = 0, \tag{6.3}$$

and hence $\psi = \psi(A)$. Similarly, since $\mathbf{E}.\mathbf{B} = 0$, one obtains $\partial(\Phi_E, A)/\partial(r,\theta) = 0$, and hence $\Phi_E = \Phi_E(A)$. Faraday's law now implies $\mathbf{E} = -\Phi'_E(A)\nabla A$, leading to the equation

$$V_\phi - \frac{\alpha}{\rho}B_\phi = (r\sin\theta)\,\Phi'_E(A), \tag{6.4}$$

where $\alpha = \psi'(A)/\mu$. Since ψ is solely a function of A (6.1) and (6.2) yield

$$\mathbf{V}_p = \frac{\alpha}{\rho}\mathbf{B}_p, \tag{6.5}$$

(cf. (3.6)), so that the poloidal components of $\mathbf{V}$ and $\mathbf{B}$ are parallel. The ϕ component of the momentum equation integrates to give

$$(r\sin\theta)\,V_\phi - \frac{(r\sin\theta)B_\phi}{\mu\alpha} = L(A), \tag{6.6}$$

which is the angular-momentum integral. The energy equation in the fixed reference frame (2.9) leads to the integral

$$\tfrac{1}{2}V^2 + \frac{\gamma p}{(\gamma-1)\rho} + \Phi_g - \frac{B_\phi\Phi'_E(A)}{\mu\alpha} = E(A), \tag{6.7}$$

whereas the entropy equation (2.3) integrates to give

$$p = K(A)\,\rho^\gamma. \tag{6.8}$$

Equations (6.3)–(6.8) are the basic integrals governing the flow, where $\Phi_E(A)$, $\psi(A)$, $L(A)$, $E(A)$ and $K(A)$ are arbitrary functions of A.

By combining the energy integral (6.7) and the angular-momentum integral (6.6), one obtains the equation

$$E_{\mathrm{rot}}(A) = \tfrac{1}{2}[V_p^2 + (V_\phi - \Omega_s r\sin\theta)^2] + \frac{\gamma p}{(\gamma-1)\rho} + \Phi_g - \tfrac{1}{2}\Omega_s^2 r^2\sin^2\theta, \tag{6.9}$$

where

$$\Omega_s(A) = \Phi'_E(A) \tag{6.10a}$$

defines the angular velocity of the plasma and

$$E_{\mathrm{rot}}(A) = E(A) - \Omega_s(A)L(A) \tag{6.10b}$$

is the energy integral in the rotating frame (see e.g. Sakurai 1985). The right-hand side of (6.9) represents the sum of the kinetic energy, enthalpy, gravitational and centrifugal potential energy of the plasma. Note that in the rotating frame $\mathbf{V}$ is parallel to $\mathbf{B}$.

It is now straightforward to solve (6.4) and (6.6) for V_ϕ and B_ϕ, to obtain

$$V_\phi = \Omega_s r\sin\theta + \frac{M_A^2(L - \Omega_s r^2\sin^2\theta)}{(M_A^2 - 1)\,r\sin\theta}, \tag{6.11}$$

$$B_\phi = \frac{\mu\alpha(L-\Omega_s r^2\sin^2\theta)}{(M_A^2-1)\,r\sin\theta}, \tag{6.12}$$

where $M_A^2 = \mu\alpha^2/\rho \equiv V_p^2/V_{Ap}^2$ defines the poloidal Alfvén Mach number. Note that for non-singular behaviour at the Alfvén surface (defined by $M_A = 1$), it is necessary that $(r\sin\theta)_A = \varpi_A = (L/\Omega_s)^{\frac{1}{2}}$, where ϖ_A is the Alfvén radius from the axis of rotation.

By taking the component of the momentum equation (2.2) parallel to ∇A (note that $\mathbf{B}.\nabla A = 0$), we obtain the trans-field momentum equation, or generalized Grad–Shafranov equation, in the form

$$\frac{\alpha}{\rho r^2\sin\theta}\left[\frac{\partial}{\partial r}\left(\frac{\alpha}{\rho\sin\theta}\frac{\partial A}{\partial r}\right)+\frac{1}{r^2}\frac{\partial}{\partial\theta}\left(\frac{\alpha}{\rho\sin\theta}\frac{\partial A}{\partial\theta}\right)\right]$$
$$-\frac{1}{\mu\rho r^2\sin\theta}\left[\frac{\partial}{\partial r}\left(\frac{1}{\sin\theta}\frac{\partial A}{\partial r}\right)+\frac{1}{r^2}\frac{\partial}{\partial\theta}\left(\frac{1}{\sin\theta}\frac{\partial A}{\partial\theta}\right)\right] = Q, \tag{6.13}$$

where

$$Q = E'(A)-K'(A)\frac{\rho^{\gamma-1}}{\gamma-1}+\frac{\alpha'}{\alpha}\frac{M_A^2(L-\Omega_s r^2\sin^2\theta)}{(1-M_A^2)^2 r^2\sin^2\theta}$$
$$-\frac{LL'}{r^2\sin^2\theta}+\frac{(L'-\Omega_s' r^2\sin^2\theta)(L-\Omega_s r^2\sin^2\theta)}{(1-M_A^2)\,r^2\sin^2\theta}, \tag{6.14}$$

(see e.g. Sakurai 1985; Heyvaerts & Norman 1989).

6.2. *The potential transonic equation*

For the special class of flows for which

$$E' = K' = \alpha' = L' = \Omega_s' = 0 \tag{6.15}$$

the trans-field equation (6.13) may be written in the form

$$\nabla\times[(1-M_A^2)\,\mathbf{B}_p] = 0. \tag{6.16}$$

It is now clear from the development of §4 that Gauss' law $\nabla.\mathbf{B}_p = 0$ may be written in the form

$$\nabla.(\sigma\mathbf{b}) = 0, \tag{6.17}$$

where

$$\mathbf{b} = \frac{\mathbf{B}_p}{\sigma B_{p0}}, \quad \sigma = \frac{1-M_{A0}^2}{1-M_A^2}, \tag{6.18}$$

and the trans-field equation (6.16) takes the form

$$\nabla\times\mathbf{b} = 0 \tag{6.19}$$

characteristic of irrotational compressible fluid dynamics.

The Bernoulli integral (6.9), as in §4, may be used to define the sound speed a of the corresponding pseudo-fluid. For flows satisfying the conditions (6.15), differentiation of the energy integral (6.9) leads to the equation

$$0 \equiv dE_{\mathrm{rot}}(A) = V_p^2\left(\frac{1}{M^2}\frac{d\sigma}{\sigma}+\frac{db}{b}+\frac{d\Phi_g}{\Phi_g}-\chi\frac{d\varpi}{\varpi}\right), \tag{6.20}$$

where

$$\varpi = r\sin\theta, \tag{6.21}$$

$$\chi = \frac{\Omega_s^2\varpi^2}{V_p^2} + \frac{M_A^2(L+\Omega_s\varpi^2)}{M_{A\phi}^2(L-\Omega_s\varpi^2)}, \tag{6.22}$$

$$M^2 \equiv \frac{b^2}{a^2} = \frac{M_A^2 M_s^2}{M_A^2+M_s^2-1+M_A^2 M_s^2/M_{A\phi}^2}, \tag{6.23}$$

$$M_{A\phi}^2 = \frac{V_p^2}{V_{A\phi}^2}, \quad M_A^2 = \frac{V_p^2}{V_{Ap}^2}, \quad M_s^2 = \frac{V_p^2}{c_s^2}. \tag{6.24}$$

In (6.18)–(6.24), $M = b/a$ is the Mach number of the pseudo-fluid with sound speed a, $\varpi = r\sin\theta$ is the radial distance from the axis of rotation (the z axis) and $V_{A\phi} = B_\phi/(\mu\rho)^{\frac{1}{2}}$ defines the ϕ component of the Alfvén velocity. The formulae (4.14) also apply in the present case, and the pseudo-fluid is supersonic in the sense $M > 1$ in the regions $V_p > V_f$ and $V_c < V_p < V_s$, but subsonic in the regions $0 < V_p < V_c$ and $V_c < V_p < V_f$, where V_f, V_s and V_c are defined in (3.23) and (3.24).

From (6.20), one finds

$$\frac{1}{\sigma}\frac{\partial\sigma}{\partial\varpi} = -M^2\left[\frac{1}{b^2}\left(b_\varpi\frac{\partial b_\varpi}{\partial\varpi}+b_z\frac{\partial b_z}{\partial\varpi}\right)+\frac{1}{V_p^2}\frac{\partial\Phi_g}{\partial\varpi}-\chi\right], \tag{6.25}$$

$$\frac{1}{\sigma}\frac{\partial\sigma}{\partial z} = -M^2\left[\frac{1}{b^2}\left(b_\varpi\frac{\partial b_\varpi}{\partial z}+b_z\frac{\partial b_z}{\partial z}\right)+\frac{1}{V_p^2}\frac{\partial\Phi_g}{\partial z}\right] \tag{6.26}$$

for the components of $\nabla\sigma/\sigma$. Using the results (6.25) and (6.26) for $\nabla\sigma/\sigma$ in the continuity equation $\nabla.(\sigma\mathbf{b}) = 0$ for $\mathbf{b}$ yields the equation

$$(a^2-b_\varpi^2)\frac{\partial b_\varpi}{\partial\varpi}+(a^2-b_z^2)\frac{\partial b_z}{\partial z}-b_z b_\varpi\left(\frac{\partial b_z}{\partial\varpi}+\frac{\partial b_\varpi}{\partial z}\right)+\frac{\chi b^2+a^2}{\varpi}\frac{\partial b_\varpi}{\partial\varpi}-\frac{b^2}{V_p^2}\mathbf{b}.\nabla\Phi_g = 0. \tag{6.27}$$

The condition $\nabla\times\mathbf{b} = 0$, (6.19), implies that b_ϖ and b_z satisfy the equation

$$\frac{\partial b_\varpi}{\partial z}-\frac{\partial b_z}{\partial\varpi} = 0. \tag{6.28}$$

Alternatively, writing $\mathbf{b} = \nabla\bar{\phi}$ results in the equation

$$(a^2-\bar{\phi}_\varpi^2)\,\bar{\phi}_{\varpi\varpi}+(a^2-\bar{\phi}_z^2)\,\bar{\phi}_{zz}-2\bar{\phi}_z\,\bar{\phi}_\varpi\,\bar{\phi}_{z\varpi}+\frac{\chi b^2+a^2}{\varpi}\bar{\phi}_\varpi-\frac{|\nabla\bar{\phi}|^2}{V_p^2}\nabla\bar{\phi}.\nabla\Phi_g = 0. \tag{6.29}$$

Equation (6.29) is the usual potential transonic flow equation for compressible irrotational non-magnetized fluid mechanics (Courant & Friedrichs 1948, chap. 1, p. 28), supplemented by the gravitational-force term ($\propto \nabla\Phi_g$), and rotational and magnetic effects ($\propto \chi$). For $M^2 > 1$ the transonic potential equation (6.29) is hyperbolic, but for $M^2 < 1$ it is elliptic.

7. Concluding remarks

In this paper we have explored the relationship between the generalized Grad–Shafranov equation or transverse force balance equation for steady MHD flows with one ignorable spatial co-ordinate and the potential transonic flow equation. The characteristics of both equations are related to the group velocity surface and Mach cone for linear magnetosonic waves emitted from a given point in the flow, in which the edge of the Mach cone corresponds to the characteristic directions. Imai's (1960) derivation of the potential transonic flow equation for magnetized flows assumed that the magnetic field was aligned with the flow. The derivation of the potential transonic flow equation in the present analysis follows from setting the effective source term in the generalized Grad–Shafranov equation equal to zero, and applies for flows that are not necessarily field-aligned.

Examples of solutions of the MHD potential transonic flow equation with an ignorable co-ordinate z for a rectangular Cartesian co-ordinate geometry were obtained by means of the hodograph transformation. Solutions corresponding to purely radial flow in the (x, y) plane, helical flows and spiral flows were investigated. The solutions obtained differ from a similar class of solutions investigated by Seebass (1961) in that the present solutions allow for components of the magnetic field and fluid velocity along the z axis not included in Seebass' analysis. The energy integral for these flows is conveniently represented as a potential-well equation in which the potential $U(\rho)$ depends only on the density. For the class of flows considered by Seebass the potential energy $U(\rho)$ equals the gas enthalpy and there is only one section to the well. By including the effect of V_z and B_z, the well splits into two parts, namely a sub-Alfvénic well with $M_A^2 < 1$ and a super-Alfvénic well with $M_A^2 > 1$. Both hyperbolic flows in which the effective Mach number $M > 1$ and elliptic flows for which $M^2 < 1$ are obtained. For hyperbolic flows the Mach number $M = V_p/c$, where V_p is the flow speed in the (x, y) plane and c is the appropriate magnetosonic speed on the Mach cone (the interpretation of M as a Mach number for elliptic flows is more problematic, since in some flows $M^2 < 0$). The Mach number M based on the generalized Grad–Shafranov equation characteristics is also the Mach number of the pseudo-fluid in Imai's analysis.

There are in general two possible super-Alfvénic flows that join at an inner limiting cylindrical radius $r = r_l$, which corresponds to a limit line of the hodograph transformation. The flows are restricted to the region $r > r_l$. The limit line occurs at the point in the flow where the radial flow speed V_r matches the phase speed c of magnetosonic waves on the Mach cone. One branch starting at $r = r_l$ consists of a superfast magnetosonic flow $(V_p > V_f)$ that accelerates with increasing r in which the density $\rho \to 0$ as $r \to \infty$. The other solution starting from $r = r_l$ consists of a near-Alfvénic decelerating flow solution with $M_A > 1$. Similarly, in the sub-Alfvénic flow regime there are two possible flows outside the limit circle $r = r_{ls}$. The two sub-Alfvénic flow solutions consist of a hyperbolic flow regime at small radii in which the flow speed V_p lies in the range $V_c < V_p < V_s$ (where V_s is the slow magnetosonic wave phase speed for waves propagating along the projected magnetic field $\mathbf{B}_p$ in the (x, y) plane; if $B_z = 0$, V_c corresponds to the slow magnetosonic group velocity for waves propagating perpendicular to $\mathbf{B}$) followed by an elliptic flow regime at larger r.

Superimposing flow potentials for purely radial and circular flow results in spiral flow solutions. The near-Alfvénic flow solutions with $M_A \approx 1$ are found to have more pronounced spiral structure than both the high-Alfvénic–Mach-number branch solutions $(M_A \gg 1)$ and the low-Alfvénic–Mach-number branch solutions $(M_A \ll 1)$. Both the projections of the streamlines and the characteristics in the (x, y) plane and in the (b_x, b_y) hodograph plane have been investigated. In the hodograph plane the super-Alfvénic characteristics for hyperbolic flow are similar to the epicycloid characteristics of pure gasdynamics (see e.g. Courant & Friedrichs 1948, chap. 4). However, the characteristics are distinctly different than both those of pure gasdynamics and those for MHD flows with $V_z = B_z = 0$ (Jeffrey & Taniuti 1964), in that a section of the characteristics extends inside the limit circle. Other solutions of the potential transonic flow equation are also possible, including magnetized versions of Ringleb flows and simple waves.

It is clear that the potential transonic flow equation with an ignorable co-ordinate can be obtained for other geometries. In particular, a derivation of the potential transonic flow equation and its relation to the generalized Grad–Shafranov equation for the case of flows with an ignorable azimuthal co-ordinate ϕ of a spherical polar co-ordinate system (r, θ, ϕ) has been carried out in §6. This geometry is probably the most suitable for models of magnetized winds (see e.g. Heinemann & Olbert 1978; Sakurai 1990).

Solutions of the generalized Grad–Shafranov equation are useful for the elucidation of the propulsion and collimation of winds and jets (see e.g. Camenzind 1986, 1987; Heyvaerts & Norman 1989; Sakurai 1990). Solutions of the potential transonic flow equation are useful for explaining aspects of MHD flow past planetary bodies (see e.g. Spreiter *et al.* 1966, 1970; Spreiter & Rizzi 1974), sub-Alfvénic flows in the solar atmosphere (see e.g. deVille & Priest 1991) and aspects of wind flows and jets. Related work by Sonnerup & Hau (1994) on field-aligned flows in CGL plasmas and by Rutkevich & Mond (1992) on magnetosonic wave propagation in spiral magnetized flows including shocks are other areas of application.

The work of G.M.W. is supported in part by NASA Grant NSG 7101. M.B. is supported in part by AFOSR under Grant F49620 92 J 0054. G.P.Z. is supported in part at the BRI by NASA SPT Program under Grant NAGW-2076. G.P.Z. is also supported in part by an NSF Young Investigator Award ATM 9357861.

This paper is Contribution 94-5 of the University of Arizona Theoretical Astrophysics Program.

Appendix

The coefficient d in the trans-field equation (3.20) takes the form

$$\begin{aligned} d = {} & E'(A)\frac{\mu\rho V_{Ap}^2}{V_p^2 - V_{Ap}^2}[V_p^2(V_p^2 - V_{Ap}^2) - \Delta] \\ & + \frac{\alpha'}{\alpha}\frac{\mu\rho V_{Ap}^2\, V_p^2}{V_p^2 - V_{Ap}^2}\left[\Delta\left(1 - \frac{V_{Az}^2}{V_p^2}\right) + V_p^2(V_{Ap}^2 + 2V_{Az}^2 - V_p^2)\right] \\ & + \Lambda'\frac{\mu\rho V_{Ap}^2}{V_p^2 - V_{Ap}^2}\left\{-V_p^2(V_p^2 - V_{Ap}^2)\left[\Phi_E' + \frac{V_{Az}^2\, V_p^2}{V_{Ap}^2(\Lambda - \Phi_E')}\right] + \Delta\left[\Lambda + \frac{V_{Ap}^2(\Lambda - \Phi_E')}{V_p^2 - V_{Ap}^2}\right]\right\} \\ & + \Phi_E''\mu\rho\, V_{Ap}^2\left[\frac{V_p^4\, V_{Az}^2}{V_{Ap}^2(\Lambda - \Phi_E')} - V_p^2(\Lambda - \Phi_E') - \frac{\Delta(\Lambda - \Phi_E')\, V_{Ap}^2}{(V_p^2 - V_{Ap}^2)^2}\right] \\ & + \frac{K'(A)}{K(A)}\frac{\mu\rho V_{Ap}^2\, c_s^2}{(\gamma - 1)\,(V_p^2 - V_{Ap}^2)}\left[\frac{\Delta}{\gamma} - V_p^2(V_p^2 - V_{Ap}^2)\right] - V_p^2 \nabla A\,.\,\nabla\Phi_g. \end{aligned} \tag{A 1}$$

REFERENCES

Camenzind, M. 1986 *Astron. Astrophys.* **156**, 137.

Camenzind, M. 1987 *Astron. Astrophys.* **184**, 341.

Courant, R. & Friedrichs, K. O. 1948 *Supersonic Flow and Shock Waves.* Springer.

deVille, A. & Priest, E. R. 1991 *Geophys. Astrophys. Fluid Dyn.* **61**, 225.

Heinemann, M. & Olbert, S. 1978 *J. Geophys. Res.* **83**, 2457.

Heyvaerts, J. & Norman, C. A. 1989 *Astrophys. J.* **347**, 1055.

Hu, Y. Q. & Low, B. C. 1989 *Astrophys. J.* **342**, 1049.

Imai, I. 1960 *Rev. Mod. Phys.* **32**, 992.

Jeffrey, A. & Taniuti, T. 1964 *Non Linear Wave Propagation with Application to Physics and Magnetohydrodynamics.* Academic.

Landau, L. D. & Lifshitz, E. M. 1987 *Fluid Mechanics*, 2nd edn. Pergamon.

Lighthill, M. J. 1960 *Phil. Trans. R. Soc. Lond.* A **252**, 397.

McKenzie, J. F. 1991 *J. Geophys. Res.* **96**, 9491.

Polovin, R. V. & Demutskii, V. P. 1990 *Fundamentals of Magnetohydrodynamics.* Consultants Bureau (Plenum).

Rutkevich, I. M. & Mond, M. 1992 *J. Plasma Phys.* **48**, 345.

Sakurai, T. 1985 *Astron. Astrophys.* **151**, 121.

Sakurai, T. 1990 *Comp. Phys. Rep.* **12**, 247.

Sears, W. R. 1960 *Rev. Mod. Phys.* **32**, 701.

Seebass, R. 1961 *Q. Appl. Maths* **19**, 231.

Sneddon, I. N. 1957 *Elements of Partial Differential Equations.* McGraw-Hill.

Sonnerup, B. U. Ö & Hau, L. N. 1994 *J. Geophys. Res.* **99**, 143.

Spreiter, J. R. & Rizzi, A. W. 1974 *Acta Astronautica* **1**, 15.

Spreiter, J. R., Summers, A. L. & Alksne, A. Y. 1966 *Planet. Space Sci.* **14**, 223.

Spreiter, J. R., Summers, A. L. & Rizzi, A. W. 1970 *Planet. Space Sci.* **18**, 1281.

Tsinganos, K. C. 1981 *Astrophys. J.* **245**, 764.

von Mises, R. 1958 *Mathematical Theory of Compressible Fluid Flow.* Academic.

Webb, G. M., Woodward, T. I., Brio, M. & Zank, G. P. 1993 *J. Plasma Phys.* **49**, 465.

Whitham, G. B. 1974 *Linear and Nonlinear Waves.* Wiley.